21963

National Library of Canada | Bibliothèque nationale du Canada

CANADIAN THESES ON MICROFICHE | THÈSES CANADIENNES SUR MICROFICHE

NAME OF AUTHOR/*NOM DE L'AUTEUR* SCHRAM GARY ROBERT

TITLE OF THESIS/*TITRE DE LA THÈSE* THE INFLUENCE OF OROGRAPHY AND SURFACE FRICTION ON SYNOPTIC SCALE VERTICAL MOTIONS OVER WESTERN CANADA

UNIVERSITY/*UNIVERSITÉ* UNIVERSITY OF ALBERT

DEGREE FOR WHICH THESIS WAS PRESENTED/ *GRADE POUR LEQUEL CETTE THÈSE FUT PRÉSENTÉE* MASTER OF SCIENCE

YEAR THIS DEGREE CONFERRED/*ANNÉE D'OBTENTION DE CE DEGRÉ* 1974

NAME OF SUPERVISOR/*NOM DU DIRECTEUR DE THÈSE* E.P. Lozowski

Permission is hereby granted to the NATIONAL LIBRARY OF CANADA to microfilm this thesis and to lend or sell copies of the film.

The author reserves other publication rights, and neither the thesis nor extensive extracts from it may be printed or otherwise reproduced without the author's written permission.

L'autorisation est, par la présente, accordée à la BIBLIOTHÈQUE NATIONALE DU CANADA de microfilmer cette thèse et de prêter ou de vendre des exemplaires du film.

L'auteur se réserve les autres droits de publication; ni la thèse ni de longs extraits de celle-ci ne doivent être imprimés ou autrement reproduits sans l'autorisation écrite de l'auteur.

DATED/*DATÉ* 20 Aug/74 SIGNED/*SIGNÉ* Gary R Schram

PERMANENT ADDRESS/*RÉSIDENCE FIXE* 19 FLAGSTONE CRESCENT
ST. ALBERT, ALBERTA

NL-91 (11-73)

THE UNIVERSITY OF ALBERTA

RELEASE FORM

NAME OF AUTHOR Gary Robert Schram

TITLE OF THESIS The Influence of Orography and Surface Friction on Synoptic Scale Vertical Motions Over Western Canada

DEGREE FOR WHICH THESIS WAS PRESENTED Master of Science

YEAR THIS DEGREE GRANTED 1974

Permission is hereby granted to THE UNIVERSITY OF ALBERTA LIBRARY to reproduce single copies of this thesis and to lend or sell such copies for private, scholarly or scientific research purposes only.

The author reserves other publication rights, and neither the thesis nor extensive extracts from it may be printed or otherwise reproduced without the author's written permission.

(Signed) Gary R Schram

PERMANENT ADDRESS:

19 Flagstone Crescent

St. Albert, Alberta

DATED 29 July 1974

THE UNIVERSITY OF ALBERTA

THE INFLUENCE OF OROGRAPHY AND SURFACE FRICTION ON SYNOPTIC SCALE VERTICAL MOTIONS OVER WESTERN CANADA

BY

© GARY ROBERT SCHRAM

A THESIS

SUBMITTED TO THE FACULTY OF GRADUATE STUDIES AND RESEARCH

IN PARTIAL FULFILMENT OF THE REQUIREMENTS FOR THE DEGREE

OF MASTER OF SCIENCE

IN

METEOROLOGY

DEPARTMENT OF GEOGRAPHY

EDMONTON, ALBERTA

FALL, 1974

THE UNIVERSITY OF ALBERTA

FACULTY OF GRADUATE STUDIES AND RESEARCH

The undersigned certify that they have read, and recommend to the Faculty of Graduate Studies and Research, for acceptance, a thesis entitled "The Influence of Orography and Surface Friction on Synoptic Scale Vertical Motions Over Western Canada", submitted by Gary Robert Schram in partial fulfilment of the requirements for the degree of Master of Science in Meteorology.

Edward Rozwski
.....
Supervisor

M. L. Khandekar
.....

Mezzacluan
.....

Date 29 July 1974

DEDICATION

To My Loving Wife, Jean

ABSTRACT

In this diagnostic study, an analysis of the three dimensional vertical motion fields associated with some selected synoptic situations over western Canada is made. A four-level model is formulated to obtain the vertical velocity fields by solution of the quasi-geostrophic omega equation. A grid encompassing western Canada including as well parts of the Northwest Territories, Alaska and eastern Pacific Ocean and a small part of the northwestern United States is used with a horizontal grid distance of 200 km in the x and y directions. Three synoptic situations were chosen so as to portray the influence of the western Cordillera of North America with particular emphasis on the initiation and development of lee cyclones over Alberta and the Northwest Territories.

With the help of the topographic charts, surface elevations at each grid point are determined. The drag coefficient at each grid point is determined by objectively interpolating Cressman's data over North America. Special consideration is given to the inadequate data network, especially over the Northwest Territories and a large part of the eastern Pacific Ocean. Data from Lark Juliet flights are included to get adequate coverage over the Pacific Ocean, while hypothetical upper air data have

been generated over several surface stations using climatological as well as observed surface data . This enabled a considerable improvement in the accuracy of the grid point data derived using an objective analysis scheme.

The influence of orography and surface friction on the vertical velocity fields is carefully evaluated by suitably changing the lower boundary conditions. The divergence and tilting terms of the vorticity equation are also calculated over selected test areas.

The incorporation of orography and surface friction through the lower boundary condition changed the vertical velocity values at 775 mb by as much as 30 percent in some areas; the influence of this lower boundary was quite small at higher levels especially at 400 mb. Further, the inclusion of the lower boundary enhanced the vorticity production on the lee side of the mountain barriers while inhibiting the same on the windward side.

The total influence of orography and surface friction appears to provide a link in the formation of lee cyclones over Alberta and the Northwest Territories.

ACKNOWLEDGEMENTS

I wish to thank Dr. Madhav L. Khandekar for his sincere interest and expert guidance throughout the term of this study. Thanks are also due to Dr. Edward P. Lozowski who served as chairman of my examining committee, and to Dr. N. Rajaratnam who in addition to Dr. Khandekar served on the examining committee.

Mrs. Laura Smith typed the final draft of this study, and cheerfully weathered the onslaught of cryptic handwritten material that I invariably produce. The technical staff of the Department of Geography drafted the base map used in this study; Mr. J. Chesterman was responsible for the excellent photo-reduction of the various charts and diagrams presented herein. Mr. D.L. Oracheski, a graduate student at this University, guided me in the interpretation of the satellite photographs, and kindly gridded one of the photographs presented in this study.

This study was conducted while I was on Educational Leave from the Atmospheric Environment Service, Environment Canada.

TABLE OF CONTENTS

		Page
DEDICATION		iv
ABSTRACT		v
ACKNOWLEDGEMENT		vii
TABLE OF CONTENTS		viii
LIST OF TABLES		x
LIST OF FIGURES		xi
CHAPTER		
I	INTRODUCTION	1
1.1	Preliminary Comments	1
1.2	Related Work	2
1.3	Outline of This Study	5
II	THE MODEL	7
2.1	The Development of the Omega Equation	7
2.2	Horizontal and Vertical Structure of the Model Atmosphere	10
2.3	Vertical Velocity Near the Earth's Surface	13
III	NUMERICAL PROCEDURES	16
3.1	The Grid	16
3.2	Finite Difference Equations	16
3.3	Solution of the Finite Difference Equations.	21
3.4	The Initial Guess Field and Lateral Boundary Condition	25

CHAPTER		Page
IV	DATA ACQUISITION AND ANALYSIS	26
4.1	Preliminary Comments	26
4.2	Analysis of Geopotential Height Data	27
4.3	Determination of the Vorticity Field	30
4.4	Determination of the Stability Factor	30
4.5	Analysis of Surface Data	31
V	RESULTS AND DISCUSSION	37
5.1	Preliminary Comments	37
5.2	Case 1 (05 January 1972: 1200 GMT)	38
5.3	Case 2 (05 March 1972: 1200 GMT)	55
5.4	Case 3 (21 May 1972: 1200 GMT)	65
5.5	Summary	69
VI	SUMMARY AND CONCLUSIONS	75
LIST OF SYMBOLS		78
STATION IDENTIFIERS		80
BIBLIOGRAPHY		81

LIST OF TABLES

Table	Description	Page
1	Static stability factors	36
2	Comparison of vertical motion values for the two lower boundary conditions: Case 1	44
3	Comparison of the tilting terms for both lower boundary conditions: Case 1	52
4	Comparison of the divergence term for both lower boundary conditions: Case 1	53
5	Comparison of the sum of the tilting term and the divergence term for both lower boundary conditions: Case 1	54
6	Same as Table 5 but for Case 2	64
7	Same as Table 5 but for Case 3	73

LIST OF FIGURES

Figure		Page
1	The basic grid area	11
2	Vertical structure of the model atmosphere	12
3	Sample grid point arrangement	17
4	Terrain height contours	33
5	Drag coefficients	34
6	Surface and 500 mb analyses: Case 1	39
7	Orographically induced vertical motion and the sum of the orographically and frictionally induced vertical motion: Case 1	41
8	Vertical motion patterns at 775 mb for the two lower boundary conditions: Case 1	42
9	Vertical motion at 600 and 400 mb for the full lower boundary condition: Case 1	45
10	Satellite photograph for Case 1	47
11	Test areas and a map of the tilting term at 775 mb: Case 1	48

Figure		Page
12	Divergence term at 775 and 400 mb (full lower boundary): Case 1	49
13	Sum of the tilting term and divergence term at 775 mb for both lower boundary conditions: Case 1	51
14	Surface and 500 mb analyses: Case 2	56
15	Vertical motion at the earth's surface and Test Areas: Case 2	58
16	Vertical motion at 775 mb for both lower boundary conditions: Case 2	59
17	Vertical motion at 600 and 400 mb for the full lower boundary condition: Case 2	60
18	Satellite photograph for Case 2	61
19	Sum of the tilting term and the divergence term at 775 mb for both lower boundary conditions: Case 2	63
20	Surface and 500 mb analyses: Case 3	66
21	Vertical motion at the earth's surface and Test Areas: Case 3	67
22	Vertical motion at 775 mb for both lower boundary conditions: Case 3	68
23	Vertical motion at 600 mb and 400 mb for the full lower boundary condition: Case 3	70

Figure		Page
24	Satellite photograph for Case 3	71
25	Sum of the tilting term and the divergence term at 775 mb for both lower boundary conditions	72

CHAPTER I

INTRODUCTION

1.1 Preliminary Comments

One of the most important parameters required to predict atmospheric motions and precipitation is the vertical component of the wind, w or omega ($\omega = \frac{dp}{dt}$ in the pressure coordinate system). Vertical motion is important on all scales of atmospheric motion ranging from thermals to synoptic scale systems. It provides the mechanism for the vertical transport of almost any atmospheric property, influencing the distribution of mass, momentum and energy in the atmosphere. Lorenz (1955) has shown that a knowledge of vertical motion patterns is necessary to determine the conversion of potential to kinetic energy and related energy transformations of the atmosphere.

On the synoptic scale the vertical velocity is only a few centimeters per second, too small for reliable measurements. For such scales of atmospheric motion it becomes necessary to estimate the vertical motion fields using computational methods applied to data gathered on other parameters. Generally, omega is estimated by using kinematic or adiabatic techniques (Panofsky, 1946)

or by the well-known omega equation, a second order partial differential equation, which can be conveniently solved by numerical methods.

The study proposed here will examine the three dimensional omega fields for some selected synoptic situations over western Canada. This will be done by solving the omega equation on a grid encompassing western Canada, including as well part of the Northwest Territories, the Yukon Territory, Alaska, the eastern Pacific Ocean, and a small part of the northwestern United States. More specifically, this study will assess the influence of the earth's orography and surface friction on the vertical motion fields in the mid-troposphere.

1.2 Related Work

The need for a diagnostic equation for vertical motion was recognized as early as 1922 by Richardson who derived what is now known as the Richardson Equation. Panofsky (1946) discussed the adiabatic and the kinematic methods for determining vertical motion. The adiabatic method utilizes the thermodynamic equation under the assumption of adiabatic flow to derive a vertical velocity equal to the adiabatic temperature change (with time) divided by the difference between the actual and adiabatic lapse rates. This technique is hampered by the lack of temperature data more frequent than at 12-hour intervals, which can lead to non-representative local temperature derivatives. The kinematic method is simple in concept, making it a very attractive method for determining vertical motion. Utilizing the continuity equation in pressure coordinates, the divergence of

the horizontal wind is integrated over a finite layer of the atmosphere. Knowing the value of omega at the bottom of the layer, omega may be easily determined at the top of the layer. Because of the basic dependence of the kinematic method on the divergence field, the method cannot be applied using a simplified non-divergent representation of the wind; it is necessary to utilize actual horizontal wind data. Errors in these data along with a minimal density in the observational network make implementation of this method difficult and as such the method has not been used extensively. However, as the density of observations increases, this method may become more useful in determination of vertical velocities. There has been a renewed interest in the kinematic method and a recent study (Smith, 1971) employs this technique to obtain vertical motion fields over eastern and central United States where the network of radiosonde stations is fairly good. However, data density over North America is still far from sufficient to permit implementation of this method on an operational basis.

Miller and Panofsky (1958) listed available techniques for determining vertical motion adding to the above the vorticity method, and the NWP (numerical weather prediction) method which makes use of the electronic computer. With the advent of electronic computers more involved equations were developed.

The first appearance of the omega type equation seems to have occurred in 1955 with Smagorinsky and Collins (1955). Fjørtoft (1955) developed a differential equation for vertical motion in the Z coordinate system which corresponded to the omega equation in the

pressure coordinate system. More recently, Cressman (1963), Stuart (1964), O'Neill (1966) and many others have used the omega equation in their studies. Smith (1971) found that results from the kinematic method can be comparable in accuracy to the results from the omega equation when certain corrections are applied.

The omega equation used by the above authors was basically adiabatic. Aubert (1957) considered the release of latent heat, incorporating this effect as a diabatic term in the omega equation. Danard (1964), following this lead, has further considered the influence of released latent heat on development, and has also considered the effect of longwave radiation as well. Smebye (1958) demonstrated that inclusion of latent heat effects for determining vertical motion is essential for precipitation computations. Thus the role of released latent heat may be quite significant in a prediction model; however, for diagnostic studies this factor may be omitted without causing any serious error.

The important influence of the Planetary Boundary Layer on the behaviour of atmospheric motions is well recognized. Newton (1956) studied the effects of surface friction on the mechanism of circulation change. He found that friction was the dominant factor during the first few hours of development. Sawyer (1959) gave a comprehensive discussion on the inclusion of terrain effects into numerical models. Cressman (1960) presented his well known chart of drag coefficients suitable for incorporating into numerical models of the atmosphere. Greystone (1962) and Danard (1969), among others, have continued along this line, demonstrating that the effects

of surface friction and orography play an important role in the dynamics of the atmosphere.

1.3 Outline of This Study

In this study, a detailed analysis of the three dimensional vertical motion fields associated with three selected synoptic situations over western Canada is performed by solving a suitable form of the omega equation as described in Chapter II. The synoptic situations are chosen so as to portray the influence of the western Cordillera of North America, with particular emphasis on the initiation and development of lee cyclones over Alberta and the Northwest Territories. The study is diagnostic in nature with the following objectives:

(a) A comparison of the three dimensional vertical motion patterns obtained with and without the orographic influence and the effects of surface friction. These effects will be introduced through a realistic lower boundary condition in the solution of the omega equation,

(b) A quantitative assessment of the influence of orography and surface friction by evaluating the divergence and the tilting term of the vorticity equation; this is done by obtaining vertical velocity fields for two different lower boundary conditions.

The details of this study are presented in the following five chapters. Chapter II outlines the development of the omega equation, together with details of the model atmosphere. Chapter III contains a brief description of the numerical procedure used in this

study. The details of data acquisition and analysis are presented in Chapter IV. The various results of this study are detailed in Chapter V, while a brief summary and conclusions make up Chapter VI.

CHAPTER II

THE MODEL

2.1 Development of the Omega Equation

The diagnostic equation for omega (ω) in a general quasi-geostrophic system can be derived from two equations:

1) An appropriate form of the vorticity equation

2) A form of the thermodynamic equation which is energetically consistent with the above vorticity equation.

The complete form of the vorticity equation in the (x,y,p,t) frame can be written, following Thompson (1961) as

$$\frac{\partial \zeta}{\partial t} + \vec{V} \cdot \nabla(\zeta+f) + \omega\frac{\partial \zeta}{\partial p} - (\zeta+f)\frac{\partial \omega}{\partial p} + \vec{k} \cdot \nabla\omega \times \frac{\partial \vec{V}}{\partial p} = 0 \qquad (2.1)$$

where ζ is the relative vorticity ($\zeta = \vec{k} \cdot \nabla \times \vec{V}$), $\vec{V}$ is the horizontal wind, f is the Coriolis parameter, and ∇ is the horizontal gradient operator.

The vorticity equation can be suitably modified under a quasi-geostrophic assumption. The quasi-geostrophic assumption, or the quasi-geostrophic filter as it is often called, is a powerful constraint between the horizontal wind and the pressure field in the free atmosphere. An explicit relationship between the horizontal wind and the pressure gradient is obtained from the divergence equation using appropriate scaling considerations. In the pressure

coordinate system the quasi-geostrophic assumption is written as

$$\vec{V}_g = \frac{g}{\bar{f}} \vec{k} \times \nabla Z \tag{2.2}$$

where $\vec{V}_g$ is the geostrophic wind, g is the acceleration due to gravity, and Z is the height of the pressure surface. The mean value of the Coriolis parameter, $\bar{f}$, is taken over the entire grid making the wind strictly rotational.

For such a filtering assumption the complete vorticity equation (2.1) reduces to

$$\frac{\partial \zeta}{\partial t} = - \vec{V} \cdot \nabla(\zeta+f) + \bar{f} \frac{\partial \omega}{\partial p}. \tag{2.3}$$

This well known form of the quasi-geostrophic vorticity equation containing a divergence term, $\bar{f} \frac{\partial \omega}{\partial p}$ has been obtained by Lorenz (1960), and used by Haltiner et al. (1963) and Stuart (1964) among many others. An expression for ζ can be determined through the geostrophic wind assumption yielding

$$\zeta = \frac{g}{\bar{f}} \nabla^2 Z \, . \tag{2.4}$$

The second equation that will be used here is the thermodynamic equation based on the first law of thermodynamics. For an adiabatic process the first law of thermodynamics is simply the conservation of potential temperature θ, which can be expressed as

$$\frac{d\theta}{dt} = 0 \, . \tag{2.5}$$

By suitable manipulation of this equation through the use of the equation of state and the definition of potential temperature we can write the following form of the thermodynamic equation in the p coordinate frame as

$$g \frac{\partial}{\partial t} \frac{\partial Z}{\partial p} + \frac{g^2}{\bar{f}} J\left(Z, \frac{\partial Z}{\partial p}\right) + \sigma\omega = 0 . \qquad (2.6)$$

Here, $\sigma = -\frac{\alpha}{\theta} \frac{\partial \theta}{\partial p}$ is a static stability factor, which is permitted to be at most a function of pressure, J is the Jacobian operator and α is the specific volume. The static stability factor specifies the stability of the atmosphere through the gradient of potential temperature along the vertical (pressure) axis and is almost always positive.

By applying the operator $\frac{\partial}{\partial p}$ to (2.3) and applying the Laplacian operator, ∇^2 to (2.6), the time dependent term can be eliminated and this yields the quasi-geostrophic omega equation as follows:

$$\sigma\nabla^2\omega + \bar{f}^2 \frac{\partial^2\omega}{\partial p^2} = g \frac{\partial}{\partial p}\left[J(Z,\eta)\right] - \frac{g^2}{\bar{f}} \nabla^2 \left[J(Z, \frac{\partial Z}{\partial p})\right] . \qquad (2.7)$$

In this expression $\eta = \zeta + f$ is the absolute vorticity. Equation (2.7) is a three dimensional partial differential equation relating omega, the vertical velocity, to two terms, namely the differential advection of vorticity in the vertical, and the Laplacian of the thermal advection. These two terms on the right hand side of equation (2.7) are typically called the forcing functions, as omega will be zero if these terms are zero.

The solution of the omega equation is most commonly obtained by numerical methods, since the analytic solution is not possible in

most cases. The usual numerical solution technique is to express the equation in finite difference form on a suitable horizontal grid covering the region of interest. Since the equation is three dimensional in nature, the atmospheric structure in the vertical direction must also be specified at some selected discrete levels. These details are given below.

2.2 Horizontal and Vertical Structure of the Model Atmosphere

The basic grid used in this study is shown in Figure 1. As mentioned in Chapter I, our main interest is to study the weather systems and their development in the lee of the Canadian Cordillera. Accordingly, the grid is approximately centered over the region of main interest, namely Alberta and parts of Northwest Territories; this helps minimize the influence of errors arising from boundary conditions over the central region of interest. More details regarding the grid size, etc., will appear in the next chapter.

The vertical structure of the model atmosphere for this study is depicted in Figure 2. The input levels of the geopotential height data for the model are at 300, 500, 700 and 850 millibars (mb), respectively. This structure, with suitable boundary conditions, allowed a solution to the omega equation to be obtained at the 400, 600, and 775 mb levels.

In order to obtain a numerical solution of the omega equation, suitable lateral and vertical boundary conditions need to be specified. Details of the lateral boundary conditions are included in the next chapter. For vertical boundary conditions, the top of the model atmosphere is assumed to be at 200 mb where omega is taken to be zero

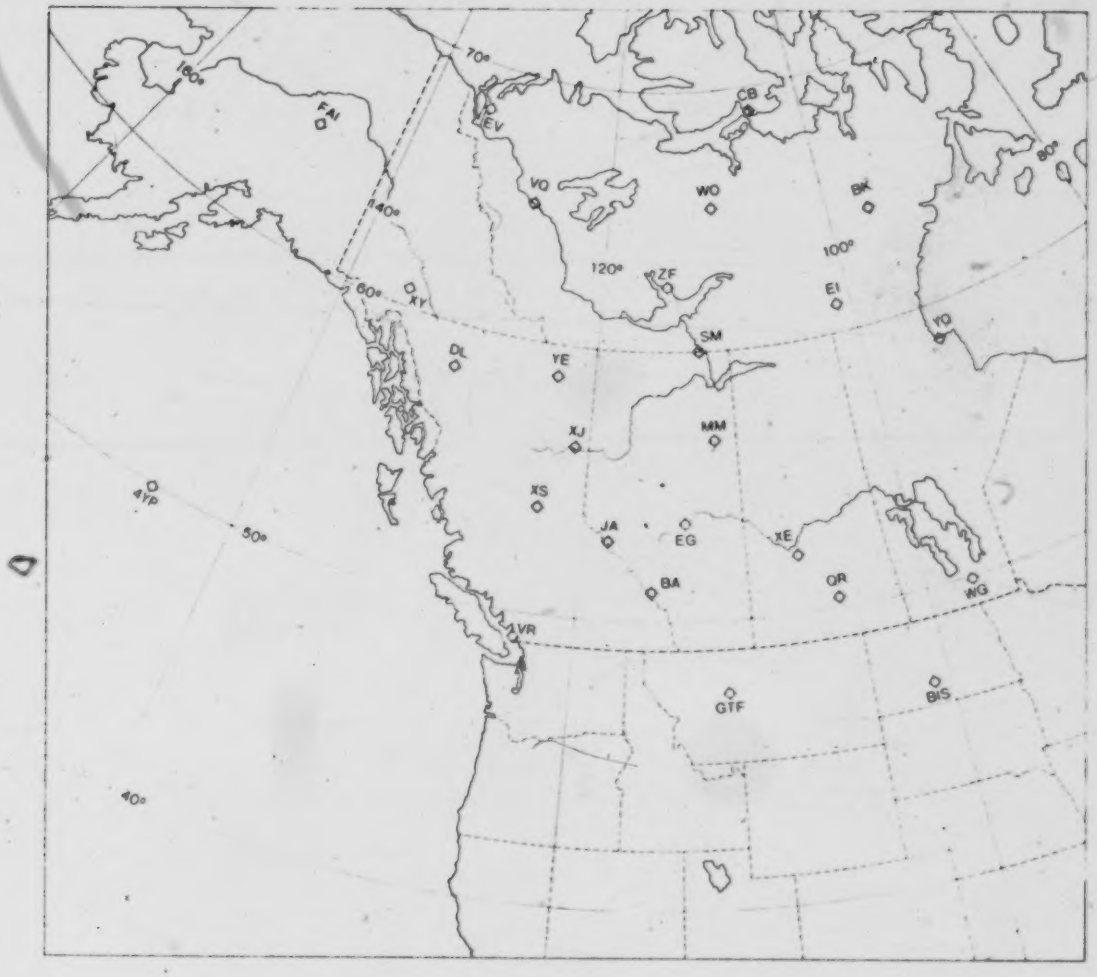

Fig. 1. The basic horizontal grid area, containing 21 rows and 23 columns (not shown). The small dot north of Edmonton (EG) used for referencing purposes only appears on all subsequent charts. See the table of symbols for a list of stations indicated by the two letter identifiers.

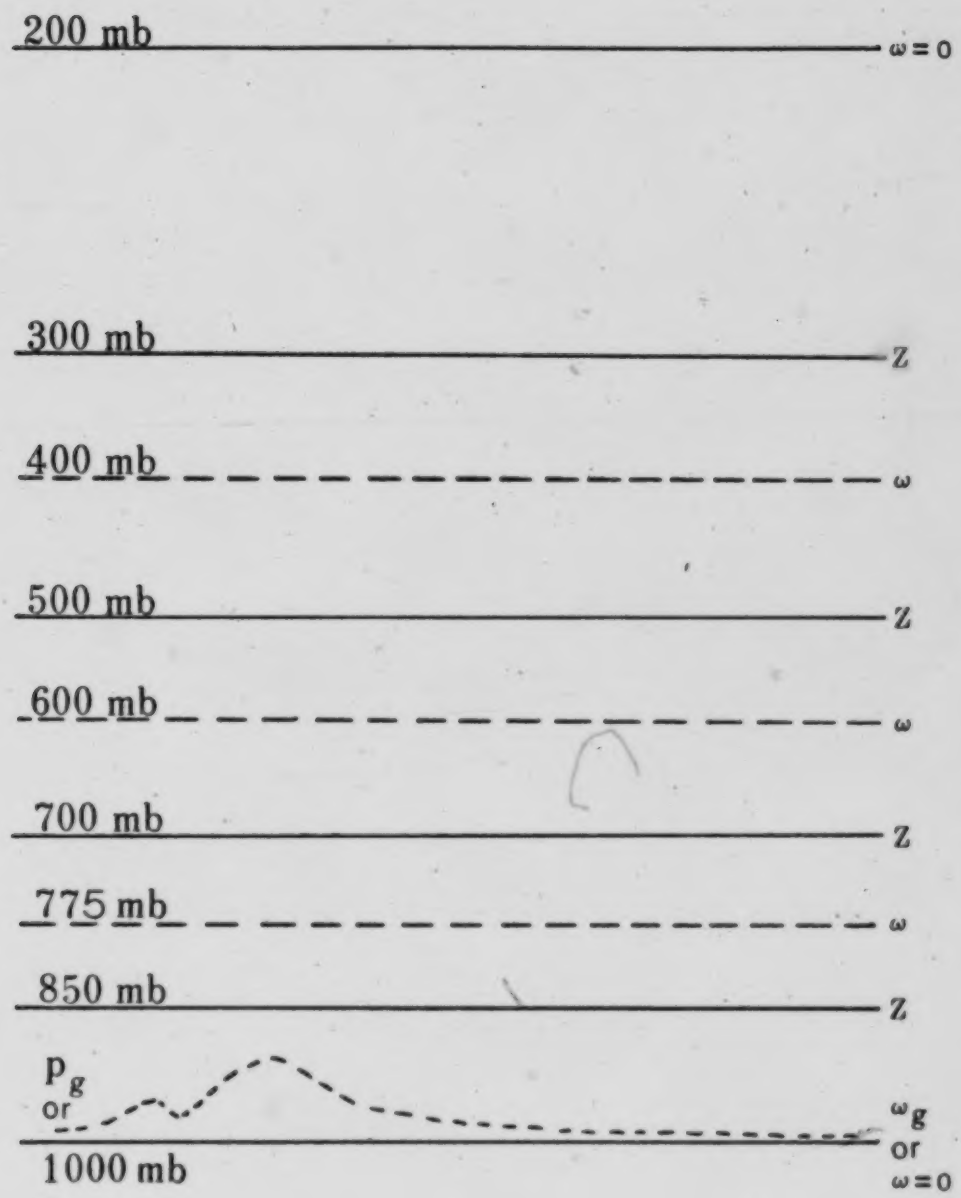

Fig. 2. The vertical structure of the model atmosphere. Geopotential height levels are labelled Z, and the omega equation solution levels are labelled ω.

everywhere. Observational and related studies show that on the synoptic scale, vertical velocity continues to diminish in the upper troposphere and becomes quite small around 200 mb or so. Similar upper boundary conditions have been utilized by Danard (1966) and others. The lower boundary condition near the earth's surface is of utmost importance for the study as it is through this condition the influence of orography and surface friction will be introduced in the omega solution. The details of the lower boundary condition are given in the following section.

2.3 Vertical Velocity Near the Earth's Surface

In general, the vertical motion near the earth's surface is mainly influenced by two factors: 1) the earth's orography (or topography) and 2) the surface friction. Both these factors contribute to the vertical velocity near the earth's surface. The contribution to vertical velocity near the earth's surface due to orography will hereafter be denoted by ω_t, while the contribution due to surface friction will be denoted by ω_f.

The terrain induced vertical motion can be obtained from the expression

$$\omega_t = -\rho_o g \vec{V}_o \cdot \nabla h \,. \quad \text{(see Haltiner, 1971)} \qquad (2.8)$$

Here, ρ_o is the density of the air at the earth's surface, $\vec{V}_o$ is the horizontal surface wind, and ∇h is the gradient or slope of the terrain height. Equation (2.8) yields the terrain induced vertical velocity in pressure coordinates.

The frictionally induced vertical motion, ω_f, can be obtained by considering ageostrophic mass transport in the friction layer or the Planetary Boundary Layer. This transport is related to the stress at the earth's surface. Above the friction layer in the free atmosphere, this stress is normally assumed to be zero.

Following Haltiner (1971) an expression relating stresses (τ_{zx}, τ_{zy}) to ω_f can be obtained as

$$\omega_f = -\frac{g}{f}\left(\frac{\partial \tau_{zy}}{\partial x} - \frac{\partial \tau_{zx}}{\partial y}\right)_o . \qquad (2.9)$$

The subscript o, denotes the terms in question to be values at the earth's surface, whereas ω_f is assumed to apply at the top of the friction layer. The friction layer may be a few hundred meters deep, but its depth is small compared to the height of the next layer in the model. Therefore the pressure at the top of the friction layer has been assumed to be the same as the pressure at the earth's surface.

Using the square relationship between surface stress and the horizontal wind

$$\vec{\tau}_o = \rho_o C_D V_o \vec{V}_o , \qquad (2.10)$$

a more appropriate expression for ω_f can be obtained by substituting (2.10) into (2.9). This yields

$$\omega_f = \frac{g}{f}\left[\frac{\partial}{\partial y}(\rho_o C_D u_o V_o) - \frac{\partial}{\partial x}(\rho_o C_D v_o V_o)\right] , \qquad (2.11)$$

where C_D is a drag coefficient relating surface stress to wind speed, and u_o and v_o are, respectively, the east-west and north-south components of the surface wind. V_o is the surface wind speed, and $\vec{V}_o$ is

the surface wind velocity vector. It should be noted that Equation (2.11) not only relates ω_f to drag, wind speed and wind direction, but also to the horizontal variation in these parameters.

The contribution to vertical motion at the earth's surface by friction and orography can be determined by taking the sum of ω_t and ω_f, as shown in the following equation

$$\omega_g = \omega_t + \omega_f \,. \tag{2.12}$$

This value of ω_g is assumed to apply at the earth's surface. As the study used pressure as the vertical coordinate, station pressures were analyzed over the grid area to determine the position of the lower boundary of the model atmosphere.

Once the upper and lower boundary values are determined, the omega equation can be solved numerically. This procedure will be described in the following chapter.

Since the main objective of this study was to evaluate in detail the influence of orography and surface friction on vertical motions, variations of the lower boundary condition were employed so as to yield suitable comparisons. More details of these variations will be discussed in Chapter V.

CHAPTER III

NUMERICAL PROCEDURES

3.1 The Grid

As mentioned earlier, a basic grid having 21 rows and 23 columns over the area of interest (see Figure 1) was used in the study. The grid spacing was 200 km in the x and y directions, true at 60N latitude on a polar stereographic projection. This basic grid together with the vertical structure of the atmosphere as defined in Figure 2 allowed the following to be obtained.

3.2 Finite Difference Equations

In order to facilitate discussions on the finite difference form of various equations, the variables were suitably subscripted as described below:

For a given grid point variable, the subscripts i,j denote respectively the row and the column of the horizontal grid containing the variable. Row numbers increase in value to the south, while column numbers increase in value to the east as indicated in Figure 3. In addition finite differencing along the vertical will involve variables at different levels. These levels will be denoted by three letters, u, c, and ℓ such that for a central level denoted by c, u and

Fig. 3. Horizontal grid point structure used in finite differencing.

ℓ will refer to the level above and below it. Reference to the levels is omitted when finite differencing involves all the variables pertaining to the same level.

For the polar stereographic projection (true at 60N) the map factor m is given by

$$m_{ij} = \frac{1 + \sin(\pi/3)}{1 + \sin(\phi_{ij})} \tag{3.1}$$

where ϕ_{ij} is the latitude of the grid point ij. At 60N the true distance between consecutive grid points is D(= 200 km) since m is equal to 1 at that latitude; at any other latitude, the true grid spacing at a grid point ij is given by

$$d_{ij} = \frac{D}{m_{ij}} . \tag{3.2}$$

For convenience, d_{ij} will be used in the finite difference expressions, thus eliminating the need for explicit inclusion of the map factor in the expressions.

The Laplacian

The best known form of the Laplacian in finite difference form is the five point Laplacian which (for a variable, ω) can be written as:

$$\nabla^2\omega_{ij} = \frac{\omega_{i+1,j} + \omega_{i-1,j} + \omega_{i,j+1} + \omega_{i,j-1} - 4\omega_{ij}}{d_{ij}^2} \tag{3.3}$$

where ∇^2 denotes the finite difference form of the Laplacian. Equation (3.3) was used wherever a Laplacian was required in a finite difference expression, except in the case of geostrophic relative vorticity.

Since this vorticity would be subject to a further finite differencing process (through the Jacobian operator) before being included in the omega equation, it was felt that the geostrophic relative vorticity should be determined as accurately as possible. Hence the nine point Laplacian written below was used for this purpose only:

$$\nabla^2 Z_{ij} = \frac{1}{6d_{ij}^2}\Big[Z_{i+1,j+1} + Z_{i-1,j+1} + Z_{i-1,j-1} + Z_{i+1,j-1} + 4(Z_{i,j+1} + Z_{i-1,j} + Z_{i,j-1} + Z_{i+1,j}) - 20Z_{ij}\Big] \tag{3.4}$$

Here, $\nabla^2 Z_{ij}$ represents the nine point Laplacian of the geopotential height field Z at a grid point ij. The use of the nine point Laplacian reduces the truncation error, which is proportional to h^4 for the nine point Laplacian and to h^2 for the five point Laplacian where h is the (normalized) grid spacing.

The Jacobian

The Jacobian of two variables, A and B, is defined as

$$J(A,B) = \frac{\partial A}{\partial x}\frac{\partial B}{\partial y} - \frac{\partial A}{\partial y}\frac{\partial B}{\partial x} \tag{3.5}$$

The corresponding finite difference form of this expression, using centered differencing is

$$J(A,B)_{ij} = \frac{1}{4d_{ij}^2}\Big[(A_{i,j+1} - A_{i,j-1})(B_{i-1,} - B_{i+1,j}) - (A_{i-1,j} - A_{i+1,j})(B_{i,j+1} - B_{i,j-1})\Big] \tag{3.6}$$

where $J(A,B)_{ij}$ is the value of the Jacobian at the grid point ij.

Using expressions (3.3) and (3.6) the finite difference analog of the right hand side of the omega equation can easily be obtained.

Finite Differencing Along the Vertical (Pressure) Axis

The finite differencing expressions for the first and second partial derivatives in the vertical direction were developed using central differences. Since the input levels and the solution levels in the model were not uniformly spaced everywhere, slight modifications were necessary to write the finite difference expressions.

For the first derivative, say $\frac{\partial \omega}{\partial p}$, the finite difference expression at a level c is

$$\left.\frac{\partial \omega}{\partial p}\right)_{ijc} = \frac{\omega_{ij\ell} - \omega_{iju}}{p_{ij\ell} - p_{iju}} \qquad (3.7)$$

This expression is assumed to be applicable at the central level. If the pressure differences between consecutive levels are equal everywhere, this expression would be valid exactly at the central level.

The second derivative $\frac{\partial^2 \omega}{\partial p^2}$ can be written as

$$\left.\frac{\partial^2 \omega}{\partial p^2}\right)_{ijc} = \frac{\frac{\partial \omega}{\partial p}_{ij\ell} - \frac{\partial \omega}{\partial p}_{iju}}{p_{ij\ell} - p_{iju}} \qquad (3.8)$$

This can be further simplified by substituting through Equation (3.7).

For the lowest level (namely 775 mb) where the omega equation is applied in the model atmosphere, finite difference expressions will involve the lower boundary conditions which are applied at the surface level. Since the surface pressure (p_g) varies from grid point to grid point, the finite difference form for $\frac{\partial^2 \omega}{\partial p^2}$ is suitably modified

to obtain

$$\left(\frac{\partial^2\omega}{\partial p^2}\right)_{ijc} = \frac{\dfrac{\omega_g - \omega_{ijc}}{p_g - p_c} - \dfrac{\omega_{ijc} - \omega_{iju}}{p_c - p_u}}{\dfrac{p_g + p_c}{2} - \dfrac{p_c + p_u}{2}} \qquad (3.9)$$

Here c refers to the 775 mb level, g the ground level and u the 600 mb level.

This equation demonstrates explicitly how the lower boundary is incorporated into the numerical solution of the omega equation, through the rate of change of divergence with respect to pressure.

3.3 Solution of the Finite Difference Equations

Using the expressions detailed in the previous section, the finite difference form of the omega equation (Equation (2.7)) is developed over the basic grid.

Since the right hand side of the omega equation involves a Jacobian as well as the Laplacian of a Jacobian, finite difference forms for these terms can be written only over the interior of the grid, excluding 2 grid points on all sides of the lateral boundary. Accordingly, there will be a matrix of 323 finite difference equations (one for each of the 17 x 19 interior grid points) involving values of omega at all interior grid points. The most convenient method of numerically solving such a set of equations is the relaxation method. In this method an initial guess field is used for the values of omega everywhere including the lateral boundary and a residual (difference between the two sides of the equation) field is constructed. This

residual field is utilized to systematically correct the initial guess field to obtain an improved field of omega values. This cycle of operation is repeated as many times as necessary till the residual field is everywhere smaller than a preassigned tolerance limit. The correction to the initial guess field can be made using a couple of different methods. The method used for this study was the well known extrapolated Liebmann procedure which can be briefly described as follows:

For the m^{th} cycle in the relaxation procedure the finite difference form of the omega equation can be written as

$$\sigma\nabla^2\omega^m_{ij} + \bar{f}^2\left(\frac{\partial^2\omega}{\partial p^2}\right)^m_{ij} - G_{ij} = R^m_{ij} \tag{3.10}$$

Here the superscript m refers to the cycle, G_{ij} is the value of the right hand side of the omega equation, often called the forcing function, and R_{ij} is the residual at the grid point ij. The superscript m does not appear in G_{ij} as the value of the forcing function does not change during the relaxation procedure.

Choosing a specific level, say 400 mb (denoted by c), Equation (3.10) is expressed in finite difference form as follows:

$$\frac{\sigma_c}{d^2_{ij}}(\omega^m_{i,j-1,c} + \omega^m_{i,j+1,c} + \omega^m_{i-1,j,c} + \omega^m_{i+1,j,c} - 4\omega^m_{ijc}) + \frac{\bar{f}^2}{(\Delta p_{ij})^2}(\omega^m_{ij\ell} + \omega^m_{iju} - 2\omega^m_{ijc}) - G^m_{ijc} = R^m_{ijc} \tag{3.11}$$

In this expression, ℓ denotes the 600 mb level while u denotes the 200 mb level and σ_c is the mean value of static stability at level c. Since $p_\ell - p_c$ is equal to $p_c - p_u$ in this case, the expression Δp_{ij}

has been used to indicate the pressure interval. Assuming R^m_{ijc} results solely from an error in ω_{ijc}, a new value ω^{m+1}_{ijc} can be defined so that

$$\frac{\sigma_c}{d^2_{ij}} (\omega^m_{i,j-1,c} + \omega^m_{i,j+1,c} + \omega^m_{i-1,j,c} + \omega^m_{i+1,j,c} - 4\omega^{m+1}_{ijc}) + \frac{\bar{f}^2}{(\Delta p_{ij})^2} (\omega^m_{ij\ell} + \omega^m_{iju} - 2\omega^{m+1}_{ijc}) - G_{ijc} = 0 \tag{3.12}$$

Subtracting Equation (3.12) from Equation (3.11) gives

$$\frac{\sigma_c}{d^2_{ij}} \left(4\omega^{m+1}_{ijc} - 4\omega^m_{ijc}\right) + \frac{2\bar{f}^2}{(\Delta p_{ij})^2} (\omega^{m+1}_{ijc} - \omega^m_{ijc}) = R^m_{ijc} \tag{3.13}$$

Solving for ω^{m+1}_{ijc} yields

$$\omega^{m+1}_{ijc} = \omega^m_{ijc} + \alpha R^m_{ijc} \tag{3.14}$$

where

$$\alpha = \frac{1}{4\left(\frac{\sigma_c}{d^2_{ij}} + \frac{\bar{f}^2}{2(\Delta p_{ij})^2}\right)}$$

is called the relaxation factor. For the standard Poisson type of equation the (normalized) relaxation factor is 0.25. This is strictly true for a two dimensional equation. Since the omega equation is three dimensional in nature and σ and Δp_{ij} in fact vary in the vertical, the relaxation factor varies slightly from level to level in the model atmosphere. Through several test runs it was found that a single value of the relaxation factor could be used for all the solution levels, permitting convergence to the solution in about 25 to 35

cycles (or scans). The optimum relaxation factor was found to vary from 0.26 to 0.32 for the three cases for which the omega equation was solved; this agrees well with similar calculations reported by Stuart and O'Neill (1967).

The computation procedure starts at the lowest level (namely 775 mb) where the omega solution is sought in the model atmosphere. As described earlier, the lower boundary condition (at the earth's surface) in the model atmosphere is incorporated in the finite difference form of the omega equation at 775 mb. Using suitable lateral boundary conditions (to be described later) and an initial guess field, the residual field is calculated beginning at the top left hand corner of the (horizontal) grid. According to the extrapolated Liebmann procedure an improved value of omega as given by Equation (3.14) is assigned to that grid point if the residual there is more than a preassigned tolerance limit. This calculation procedure is repeated at the next grid point in the row and in this way the entire grid at one level (775 mb) is scanned. Having scanned one level, the calculation proceeds to the next level (namely 600 mb) where the omega solution is required. Using an equation similar to (3.10) the entire grid is scanned as before and improved values of omega are obtained. Finally the calculation proceeds to the topmost level (which is 400 mb) where the omega equation is applied and a similar procedure is carried out.

Once an improved guess field of omega is obtained at all the three levels, the calculation procedure returns to the lowest level for the next cycle. This chain of operations is continued until the residuals at all grid points at all three levels are within

the prescribed tolerance limits. The tolerance limit was set at two to three orders of magnitude smaller than the typical magnitude of the forcing function of the omega equation.

3.4 The Initial Guess Field and Lateral Boundary Conditions

As a forerunner to the determination of the guess field the grid point values of the orographically and frictionally induced vertical motion (ω_g) were calculated. The initial guess field was set as 0.75 ω_g at 775 mb, 0.5 ω_g at 600 mb and 0.25 ω_g at 400 mb. This included values of omega at the lateral boundary as well as over the interior grid. As mentioned previously, these edge values did not change in subsequent sweeps as the omega equation was not solved at the edges of the grid due to the nature of the finite difference equations. These edge values then formed the lateral boundary conditions for the solution of the omega equation. Some experimentation with the lateral boundary showed that a somewhat more sophisticated lateral boundary condition did not significantly change the solution.

In order to follow this numerical procedure, data at various levels of the model atmosphere are required to yield the omega solution. The acquisition and analysis of these input data will be discussed in the next chapter.

CHAPTER IV

DATA ACQUISITION AND ANALYSIS

4.1 Preliminary Comments

The data required to solve the omega equation can be placed in two categories:

1) geopotential height data

2) data pertaining to the lower boundary.

Most of this information was obtained from the Northern Hemispheric Data Tabulations (NHDT) which were available from the National Climatic Centre in Asheville, North Carolina, U.S.A. The information was in the form of radiosonde reports for upper air data and coded synoptic reports for surface data. Grid point data of terrain height were abstracted from maps available in the Map Library of the Department of Geography at this University; an objective format was used to ensure that the data abstraction was consistent from grid point to grid point. The grid point values of the drag coefficient were obtained by suitably re-analyzing a map of drag coefficients supplied by Dr. Cressman of the National Oceanic and Atmospheric Administration (NOAA) in Washington, D.C., U.S.A.

The following sections will detail the procedures used to analyze these data.

4.2 Analysis of Geopotential Height Data

Grid point values of the geopotential height data were required in order to calculate the absolute vorticity as well as advection terms in the forcing function of the omega equation.

Until the advent of electronic computers, maps of the geopotential height field were analyzed subjectively. Although this type of analysis can be performed quite accurately, there is always a possibility of variation in analysis technique from person to person. On the other hand, a computer can be utilized to produce maps based on a suitable objective analysis scheme. Such a procedure always ensures a consistent map analysis free of human bias.

In this study a computer program developed by Glahn and Hallenbaugh (1969) was employed to analyze the geopotential height data over the grid area. This method is basically similar to that used by Bergthorssen and Döös (1955) and Cressman (1959). The analysis method is one of successive approximations, embodying the geostrophic wind relationship (Equation 2.2), permitting the use of geopotential heights and reported winds in adjusting the "first guess" of the geopotential height field analysis. The method involves a series of sweeps or passes over the data. On each sweep, a correction is made to all grid points within a radius of R grid intervals from an observation; R is called the radius of influence. R varies with each sweep, normally decreasing in value as the analysis becomes more refined. Any errors in the observations are detected through a process which compares the grid analysis to the station report. The geopotential height or the wind (or both) can be judged to be in

error if the analysis and the observation differ by more than a certain predetermined error limit. In such a case the observation is not used to make corrections to the analysis during the sweep in question. The observation may be accepted again on subsequent sweeps if the observation and the analysis come into better agreement. Smoothing was performed on the final sweep in order to remove wavelengths less than twice the grid interval (about 400 km) from the analysis. Such wavelengths can lead to instabilities in numerical computations. Approximately one hundred radiosonde reports were available for the grid area and vicinity. Additional data at 500 and 300 mb levels were available (in Case 1) from the weather reconnaissance flight Lark Juliet, operated by the United States Air Force. These data were extremely useful for analysis purposes over the eastern Pacific Ocean and the Gulf of Alaska, where the flight operates.

With the Lark Juliet data as an exception, very few observations were available over the Pacific Ocean; a similar problem existed over the eastern half of the Northwest Territories. To ensure that the analysis scheme would not develop any serious errors it was necessary to introduce synthetic (or bogus) observations over these data-sparse regions. This bogussing process is performed routinely in most operational analysis methods. Geopotential heights were bogussed over the Pacific Ocean at 850, 700, 500 and 300 mb using a method described by Whitehead (1965), which develops the heights on the basis of observed surface pressure and temperature; this surface information was available from Marine Synoptic reports. The method determines the geopotential heights on the assumption that

the atmosphere is hydrostatic with a linear lapse rate of temperature. The lapse rate is determined by assuming that the density of the atmosphere coincides with that of the standard atmosphere at some height above the surface. This height was assumed to be the scale height of the atmosphere (about 8 km). A modification of this method was used to obtain (bogus) geopotential heights over the land stations. The modification essentially consisted of adding the elevation above sea level of the station to the derived heights; the original assumption of the scheme was that the station was at sea level. Land bogus stations were located at Ennadai Lake (EI) and Contwoyto Lake (WO), both in the eastern half of the Northwest Territories, and at Saskatoon, Saskatchewan (XE). The bracketed letters are the code letters used to identify the station in normal weather office operations. The actual locations of these stations can be seen in Figure 1. The bogussing scheme was also performed at locations where a radiosonde report was available, in order to determine the error in the bogussing system for the particular meteorological situation under consideration. It was assumed that a similar error would be present at bogus stations within a reasonable distance from the actual observations, and an appropriate adjustment was made to the bogus report. Bogus values were also considered in light of careful hand analyses and computer analyses from the Canadian Meteorological Centre at Dorval, Quebec.

The objective analysis procedure with the bogus data included results in quite reasonable analyses of geopotential heights. Mean deviations of the analyzed geopotential height fields from the observed data were approximately 5 m at 850 and 700 mb, 10 m at 500 mb and 15

to 20 m at 300 mb. Part of the larger deviations at 500 and 300 mb were due to the fact that verification procedure compared the analysis to observations even though the observations had been rejected by the analysis routine.

4.3 Determination of the Vorticity Field

Values of the geostrophic relative vorticity ζ were obtained at 850, 700, 500 and 300 mb using the nine point Laplacian of the analyzed geopotential height field. As mentioned in Chapter III the nine point Laplacian was used in order to obtain a greater accuracy in the vorticity values. The absolute vorticity η can be obtained simply by adding f the Coriolis parameter to the relative vorticity. Even though care was taken to ensure accuracy in the geopotential height analysis, a few areas of negative absolute vorticity appeared. This may have been caused by the geostrophic assumption in the height analysis program. However, it is also possible that the absolute vorticities in these areas were indeed negative. Mogil and Holle (1972) have discussed the implications of anomalous winds and negative vorticities. In any event, these negative (vorticity) areas were quite small, and were not considered to be a serious problem.

4.4 Determination of the Stability Factor

The stability factor $\sigma = -\frac{\alpha}{\theta}\frac{\partial\theta}{\partial p}$ was evaluated using the radiosonde reports from the NHDT for each of the stations used in analyzing the height fields. The factor was calculated at the solution levels for the omega equation, namely 775, 600 and 400 mb. For each

case, a mean value of σ was determined at each of the three levels, in keeping with the assumptions made in section 2.1. These mean values were used in the numerical solution of the omega equation. The static stability at 400 mb was generally larger than the values at the other two levels as shown by Gates (1961). Individual values of static stability varied more widely from location to location than first expected; the most marked departures from the mean values occurred at the northern Canadian observing sites. Mean values of static stability used in the solution of the omega equation are presented in Table 1. (See page 36.)

4.5 Analysis of Surface Data

Several parameters pertaining to meteorological conditions at the earth's surface were required in order that Equations (2.8) and (2.11) could be used to determine the vertical motion at the top of the friction layer. These are:

1) Surface winds
2) Surface station pressure
3) Surface temperature.

In addition, grid point values of the terrain height were required so that orographically induced vertical motion could be determined for use in Equation (2.8). Both these equations also require ρ_o, the surface density. This was determined using the equation of state, $p_o = \rho_o R_d T_o$, where R_d is the gas constant for dry air. Grid point values of the surface pressure P_o and surface temperature T_o were used in conjunction with R_d to obtain grid point values of ρ_o.

Terrain Height Data

The height of the terrain above sea level, for each of the 483 grid points was obtained by hand in an objective manner, using World Aeronautical Charts (1:1,000,000 in scale). These charts are published in Canada by the Surveys and Mapping Branch, Department of Energy, Mines and Resources and in the United States by the U.S. Coast and Geodetic Survey and the United States Army Corps of Engineers. Twenty-five grid points within a circle of radius 100 km centered over a grid point were analyzed by eye; the points were so distributed so as to yield higher weightage to the values near the grid point in question. The (simple) mean value of these 25 points was taken to be the value of the terrain height for that grid point. A plastic overlay drawn to the appropriate scale was used to ensure consistency in placing the twenty-five points on the map relative to the grid point. Figure 4 depicts the analyzed terrain height data as obtained over the grid. Height gradients were calculated from these data using centered finite differencing methods. The gradients were then used in Equation (2.8) along with surface density to obtain ω_t, the orographically induced vertical motion at the earth's surface.

Drag Coefficient Data

Drag coefficient data (supplied by Dr. Cressman of NOAA) were re-analyzed to the 200 km grid from the original 381 km grid using biquadratic interpolation. Figure 5 is a map of these drag coefficients for the grid used in this study. Unless otherwise indicated on this map, the value of the drag coefficient is 1296×10^{-6} (dimensionless).

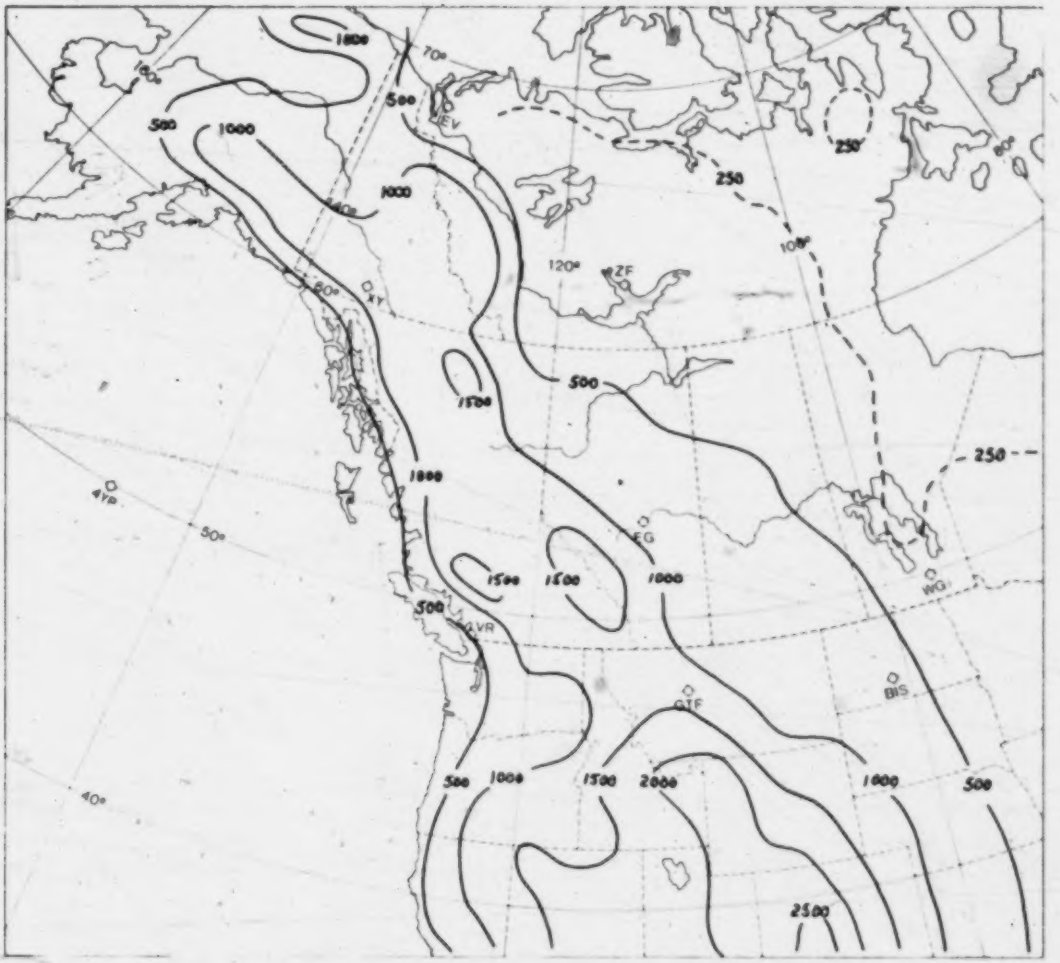

Fig. 4. Analysis of the grid point terrain height data. Units are meters (m).

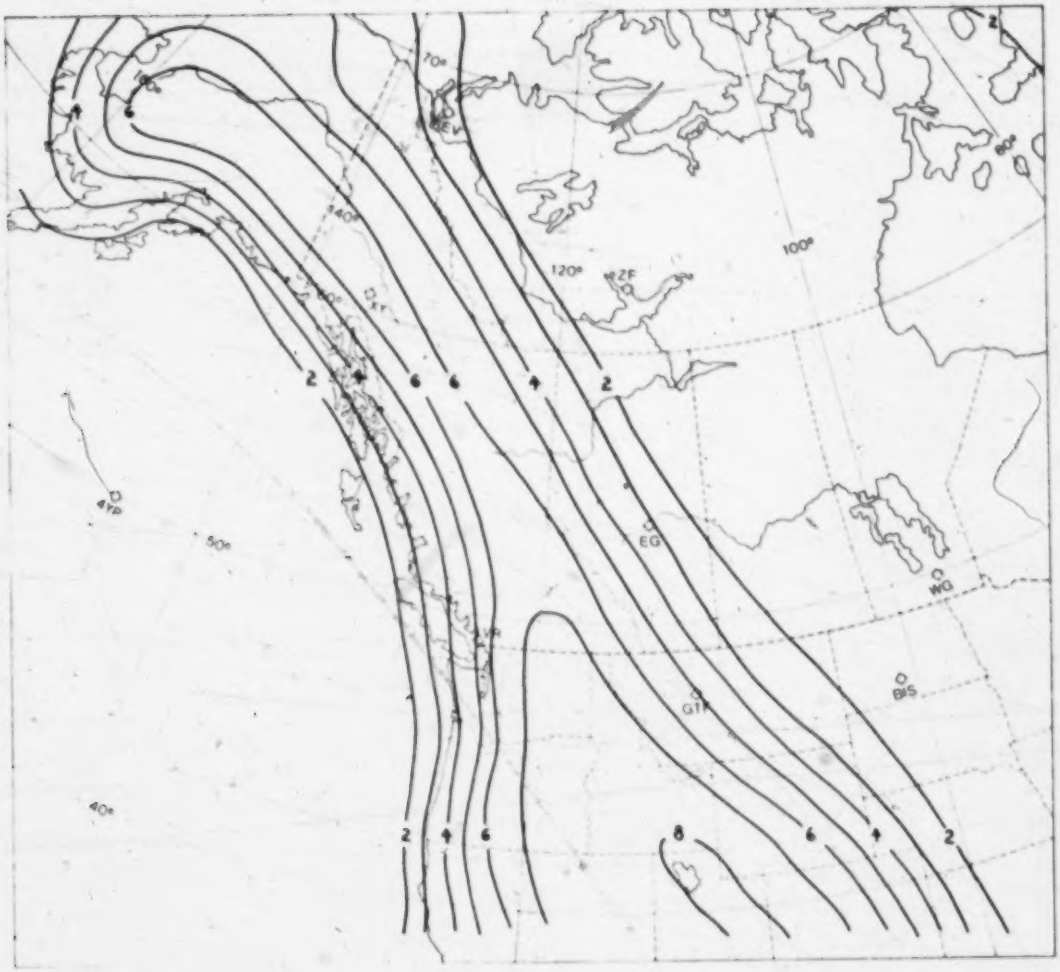

Fig. 5. Analysis of drag coefficients. Units are 10^{-3} (dimensionless).

Objective Analysis of Surface Wind, Pressure and Temperature

The network of stations reporting surface data is of course much more dense than that of radiosonde data. Approximately 300 surface reports were available for each case. An objective analysis program outlined by Glahn, Hollenbaugh, and Lowry (1969), originally designed to analyze sea level pressures, was modified slightly to analyze station pressure, observed surface winds, and station temperatures. All these data were available from the synoptic sequences listed in the NHDT. The objective analysis system interpolated surface data to the grid points using Bessel's Interpolation Formula which is biquadratic in nature. In areas where the gradient of station pressure (in particular) was strong, the biquadratic interpolation scheme had difficulty in properly fitting the data to the grid. A slight modification of the computer program counteracted this problem, greatly improving the analyses in these areas.

In spite of a large number of surface observations, bogus data were necessary over the Pacific Ocean since data over the ocean were generally sparse with most marine reports being concentrated along shipping routes. The bogus data were introduced after a careful inspection of surface weather charts, kindly supplied by the Edmonton Weather Office and the Arctic Weather Office, both located at Edmonton, Alberta.

The same analysis technique was used to analyze station temperature and observed surface winds (in component form). These analyzed fields were then used in determining the field of ω_f and ω_t which were added to obtain ω_g, the total vertical motion at the

earth's surface. With grid point values of station pressure analyzed, the lower boundary was incorporated into the model atmosphere as outlined in section 3.2, and the omega equation was solved numerically. The results are presented in the next chapter.

	775 mb	600 mb	400 mb
Case 1	.000255	.000238	.000493
Case 2	.000221	.000232	.000460
Case 3	.000176	.000199	.000379

Table 1. Values of the static stability factor used in the solution of the omega equation. Units are gm^{-2} cm^4 sec^2.

CHAPTER V

RESULTS AND DISCUSSION

5.1 Preliminary Comments

In order to explicitly evaluate the influence of surface friction and orography on vertical motion, two distinctly different lower boundary conditions were chosen to yield suitable comparisons. The first, a simple lower boundary, consisted of the surface station pressure set at 1000 mb everywhere over the grid, with the vertical motion at the earth's surface set to zero. This condition represented a flat, frictionless surface. The second boundary condition called the full lower boundary consisted of the objectively analyzed surface station pressures, along with the vertical motion at the earth's surface in response to both orography and surface friction. This boundary condition thus incorporates the effect of the earth's irregular surface in general and that of the western Cordillera in particular on the vertical motion fields.

For quantitative comparison, the tilting term $(-\vec{k} \cdot \nabla\omega \times \frac{\partial \vec{V}}{\partial p})$ and the divergence term $(\zeta+f)\frac{\partial \omega}{\partial p}$ of the full vorticity equation were evaluated using the omega fields obtained with the two different lower boundary conditions. These two terms indicate the change in

vorticity with time following a parcel of air, and are baroclinic in nature. It may be recalled that in the quasi-geostrophic formulation of the omega equation, only the divergence term is included while the tilting term is dropped out of the vorticity equation because of scaling considerations. Consequently, the calculations made here are meant to provide (at least) a first approximation to the actual magnitudes of the tilting and the divergence terms. Because of the importance of these baroclinic terms in vorticity production, a detailed assessment of these terms was done over selected test areas for each case; this procedure provided a quantitative evaluation of the influence of orography and surface friction. The various results for each of the three chosen cases are described in the following sections.

5.2 Case 1 (05 January 1972: 1200 GMT)

The various results for Case 1 are presented in Figures 6 to 13 and Tables 2 to 5. Figure 6 shows the surface analysis for Case 1 along with the 500 mb geopotential height analysis, including the absolute vorticity pattern. At the surface a deep (964 mb) low pressure system moving slowly eastward was situated in the Gulf of Alaska. Satellite photographs received at the University of Alberta showed that the system was occluded at this time. In addition a lee trough was established at the surface over Alberta. At 850 mb (not shown) a similar pattern existed with major areas of warm air advection present over the southern Yukon and over northeastern Alberta. At 500 mb a ridge was present along a line through central British

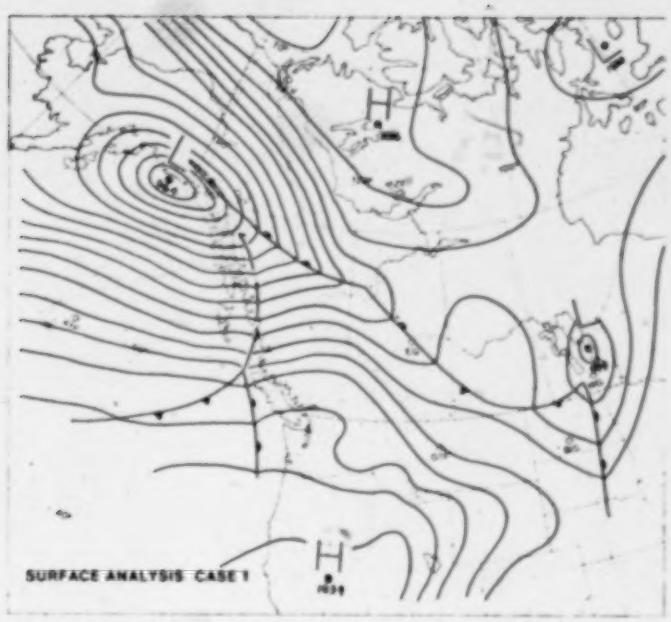

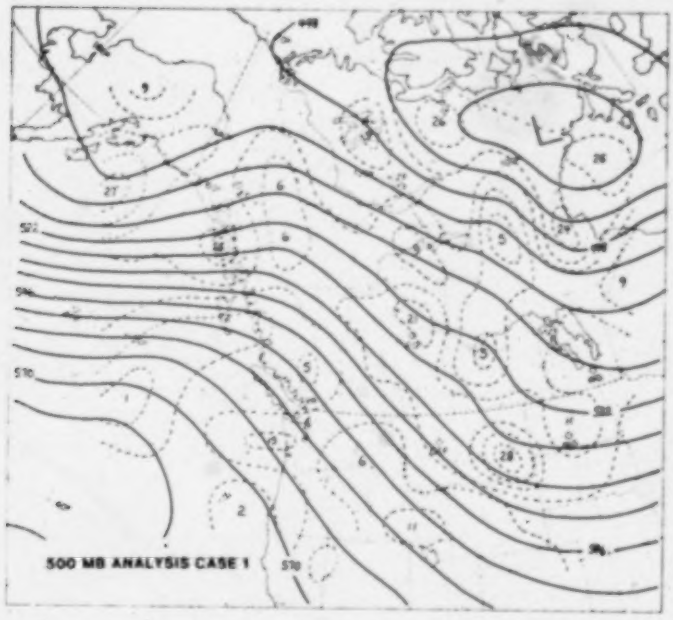

Fig. 6. Surface analysis and 500 mb analysis including absolute vorticity for Case 1 (05 January 1972, 1200 GMT). Pressures are in mb, geopotential heights in decameters, and vorticity units are 10^{-5} sec^{-1}.

Columbia (B.C.) to the southern Yukon; the airflow was west-southwesterly west of the ridge and northwesterly to the east of the ridge, over Alberta. A major area of positive vorticity advection (PVA) was present over the Alaskan Panhandle with a weaker area of PVA over Lake Athabasca. Twelve hours later a new low (with central pressure 985 mb) developed in northeastern Alberta, while the Gulf of Alaska low had drifted inland and filled drastically.

Figure 7 shows the analyses of orographically induced vertical motion and the sum of orographic and frictionally induced vertical motion (denoted ω_{T+F} on the figure). As expected, a major area of ascent was situated along the west coast, while subsidence prevailed along the eastern slopes of the Rocky Mountains through most of Alberta into the United States. Ascent of up to 5 cm sec^{-1} was noted over the Alaskan Panhandle. Descent of approximately 1 cm sec^{-1} was present along the eastern slopes of the Rocky Mountains in Alberta, increasing to 3 cm sec^{-1} over Wyoming. A comparison of these two analyses reveals that ascent on the west coast was enhanced by about 25 percent as a result of inclusion of frictional effects into the calculation. A similar but lesser effect occurs on the subsidence pattern along the eastern slopes of the Rockies. In areas of relatively even terrain the effect of including friction resulted in changes which were generally an order of magnitude less than the values of vertical motion induced by orography alone.

Figure 8 shows the vertical motion patterns obtained at the 775 mb level using the simple and the full lower boundary conditions. Ascent over the Alaskan Panhandle increased 25 to 30 percent when the full boundary was included. Ascent decreased

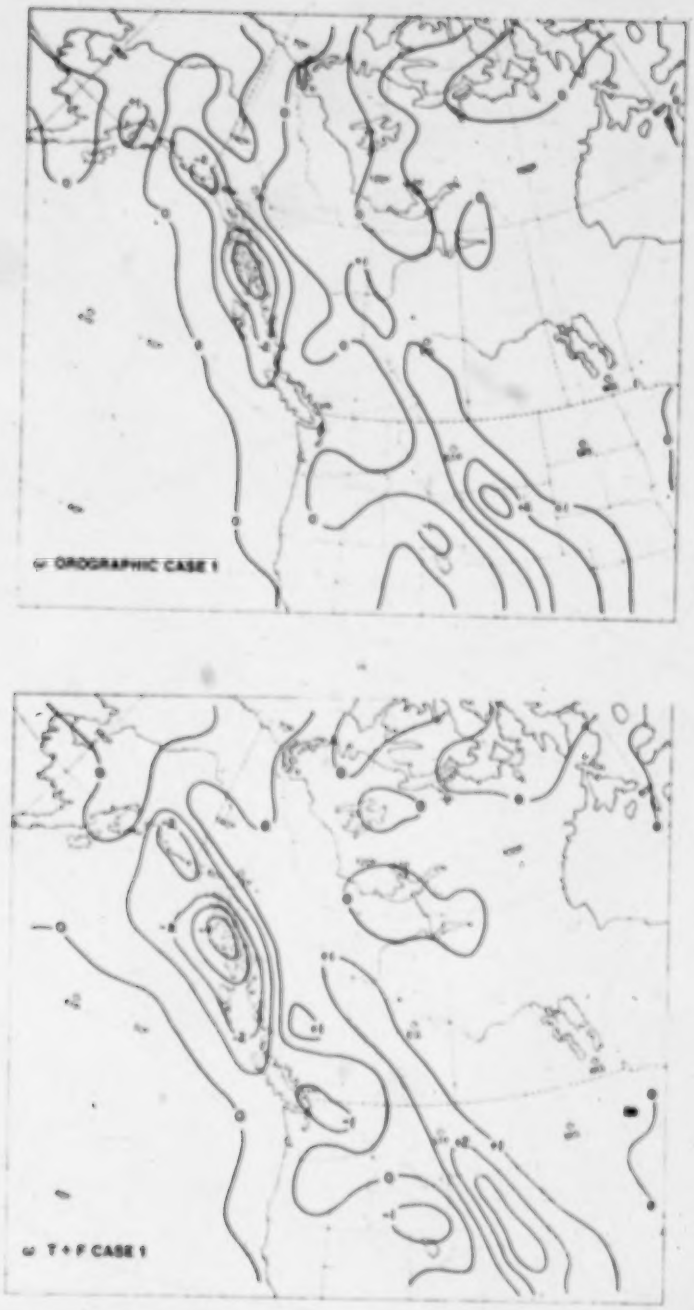

Fig. 7. Orographically induced vertical motion (OROGRAPHIC) and the sum of orographically and frictionally induced vertical motion (ω T+F). At this level $w \doteq -0.9\,\omega$, where w is the vertical velocity in cm sec^{-1} and ω is the vertical velocity in microbars sec^{-1}. Negative values of omega denote ascent and positive values of omega denote subsidence.

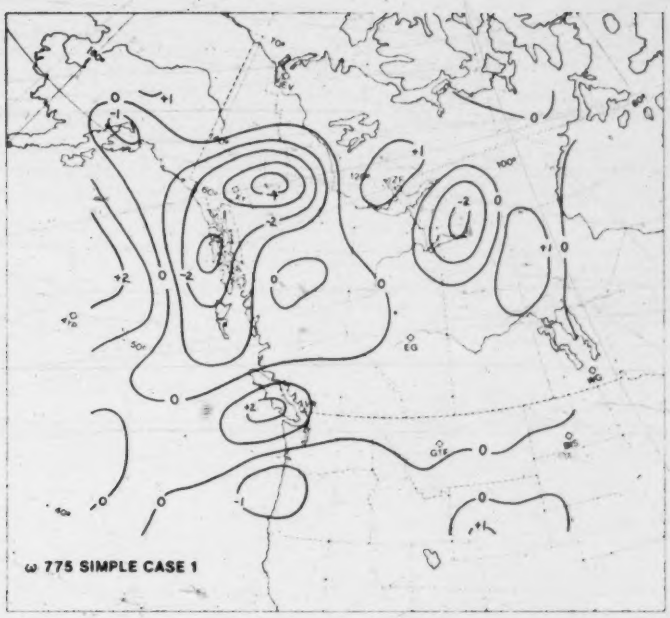

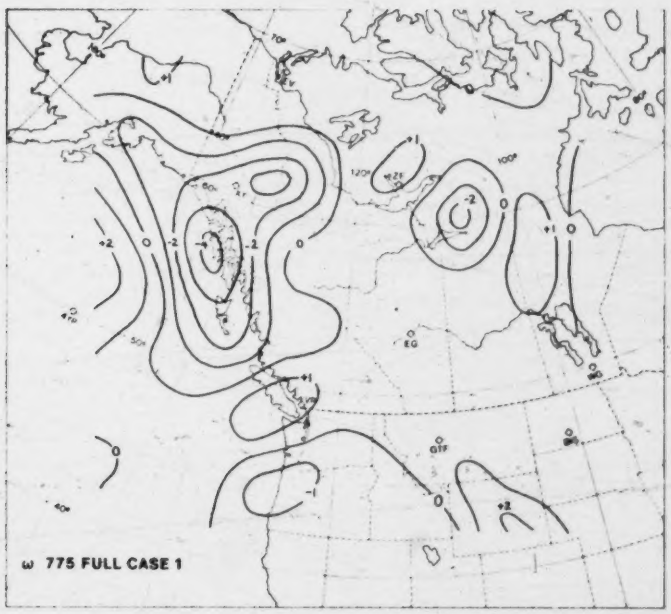

Fig. 8. Vertical motion patterns at 775 mb obtained using the two different lower boundary conditions. At this level $w \doteq -1.1\,\omega$.

somewhat over the southern Yukon. Little change in the ascent pattern over Lake Athabasca occurred when the full boundary was included; this is logical, since the terrain in that area is relatively flat, and there is little variation in surface friction.

Table 2 demonstrates effectively the differences in omega values at the three solution levels obtained with the two different lower boundaries. These values of omega refer to the ninth row of the grid running from the Alaskan Panhandle to the vicinity of Lake Athabasca (see Figure 11). The differences in omega values are quite significant at the 775 mb level where the inclusion of the full boundary changes the values by as much as 30 percent at some grid points. As would be expected, the lower boundary exerts a diminishing influence on the omega solution at higher levels, especially at 400 mb.

Figure 9 shows the vertical motion patterns at the 600 and 400 mb levels using the full lower boundary conditions. The corresponding vertical motion patterns using the simple lower boundary are not shown since they are basically similar to those of Figure 9. These vertical motion patterns agreed well with the reported surface weather phenomena at the analysis time. A large area of precipitation (snow) existed in northern B.C. and the Yukon, correlating with the ascent pattern in those areas. Also, a separate area of snow over Lake Athabasca was in phase with the separate area of ascent shown on the vertical motion analyses. Figure 10 is the satellite photograph of the weather pattern mainly over the Pacific Ocean and B.C., taken about eight hours after the analysis time

BOUNDARY										
					775 mb					
Full	-4.4	-2.4	-0.2	0.2	0.3	0.3	0.1	-0.1	-1.3	-0.6
Simple	-3.2	-1.9	-0.5	-0.2	0.0	0.1	0.1	-0.2	-1.4	-0.7
					600 mb					
Full	-3.3	-2.9	-1.9	0.3	0.2	0.1	0.2	-0.3	-2.1	-0.8
Simple	-2.9	-2.8	-2.0	0.1	0.0	0.0	0.1	-0.4	-2.1	-0.9
					400 mb					
Full	-1.6	-2.5	-1.1	0.1	-0.7	-2.0	-0.8	-0.6	-0.5	0.0
Simple	-1.4	-2.5	-1.1	0.1	-0.8	-2.1	-0.8	-0.7	-0.6	-0.1

Table 2. Values of omega (Case 1) taken from row 9 of the grid columns 8 to 17 (see Fig. 11). Values are shown for each solution level for both lower boundary conditions. Units are microbars per sec.

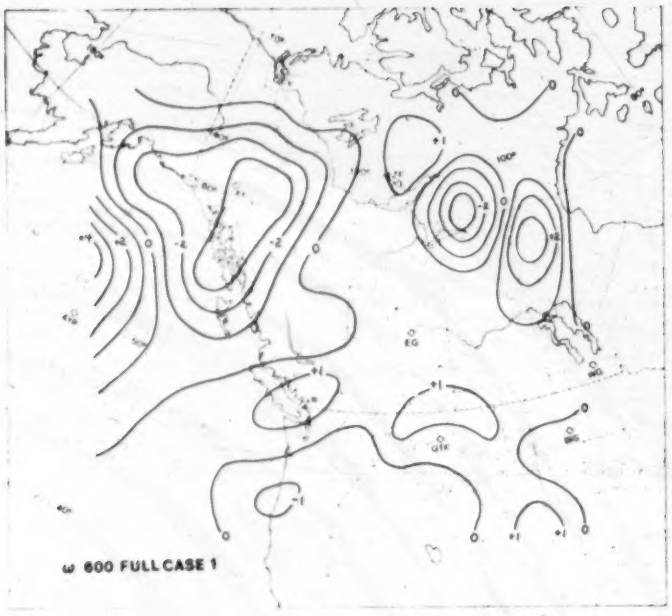

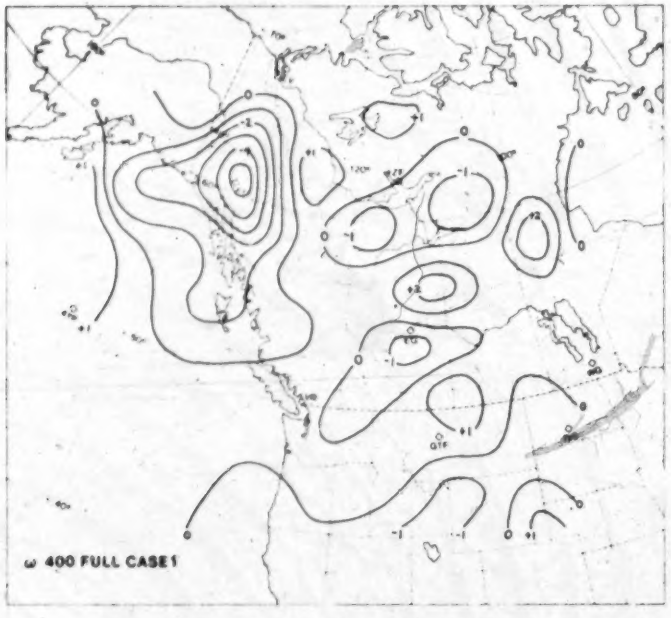

Fig. 9. Vertical motion patterns at 600 mb and 400 mb obtained using the full lower boundary. At 600 mb, $w \doteq -1.27\ \omega$. At 400 mb, $w \doteq -1.77\ \omega$.

(1200 GMT). The photograph demonstrates effectively that the Gulf of Alaska low was occluded, and shows extensive cloud cover over Vancouver Island and central B.C.

The top half of Figure 11 shows the test areas used in this case for comparison of the baroclinic terms, namely the divergence and tilting terms of the vorticity equation at various levels in the atmosphere. Area 1 was chosen to demonstrate the effect of the eastern slopes of the Rocky Mountains, and Area 3 to show the effect of the sharply rising terrain on the west coast on the baroclinic terms. Area 2 was chosen mainly because a great deal of ascent was occurring in that area. Area 4 was chosen because the terrain was flat in that area, and also because the new low developed on the western boundary of that area. The test areas in all three cases contained an average of 20 grid-points.

The bottom half of Figure 11 shows an analysis of the tilting term at 775 mb using the omega field derived incorporating the full boundary. Positive values indicate that parcel vorticity is increasing with time; the reverse is true for negative values. Note that the tilting term is most active in areas of frontal activity (see surface analysis).

Figure 12 shows the analyses of the divergence term at 775 mb and 400 mb derived from the omega fields using the full boundary. Again, positive values indicate parcel vorticity increasing with time (convergence) and negative values indicate parcel vorticity decreasing with time (divergence). At 775 mb, as expected, convergence appears in the vicinity of the Gulf of

Fig. 10. Satellite photograph of the meteorological situation for Case 1. The Queen Charlotte Islands are visible in the right center of the photograph, with the occluded low at the top centre. The photograph was taken by the ESSA-8 weather satellite about 2000 GMT, 05 January 1972, about ten hours after analysis time.

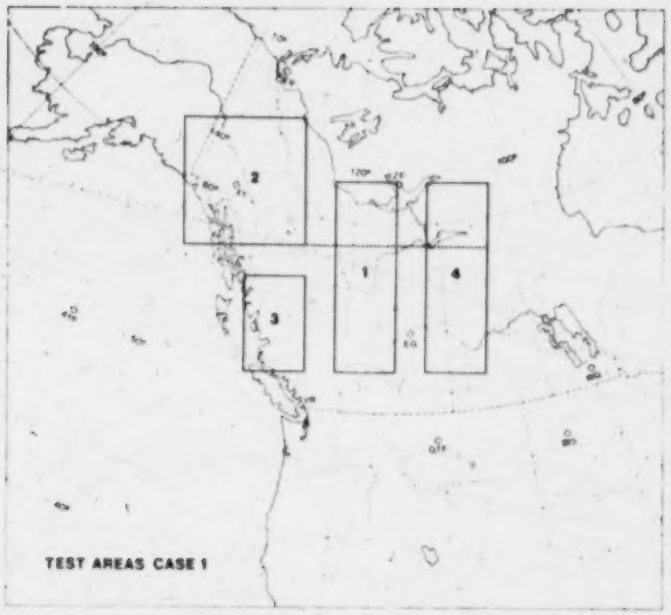

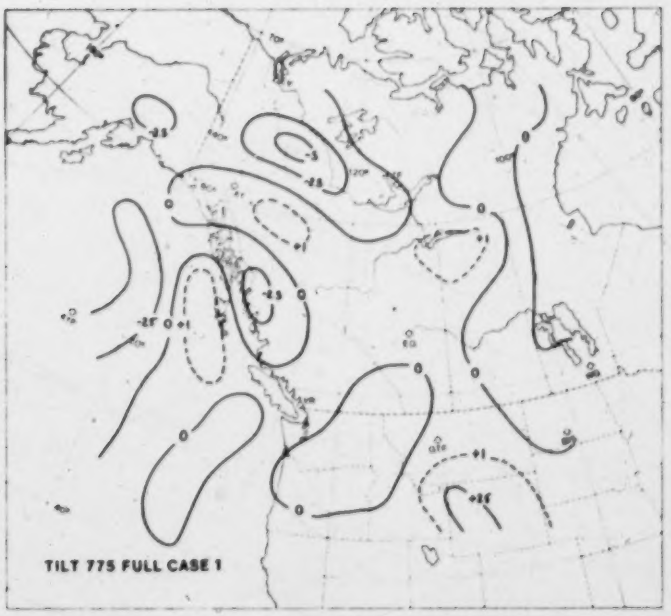

Fig. 11. Test areas and an analysis of the tilting term (TILT) at 775 mb for the full lower boundary condition. Units of the tilting term are 1.25×10^{-10} sec^{-2}. The dotted line in the test area diagram is part of row 9 of the grid from which sample omega values were taken (Table 2).

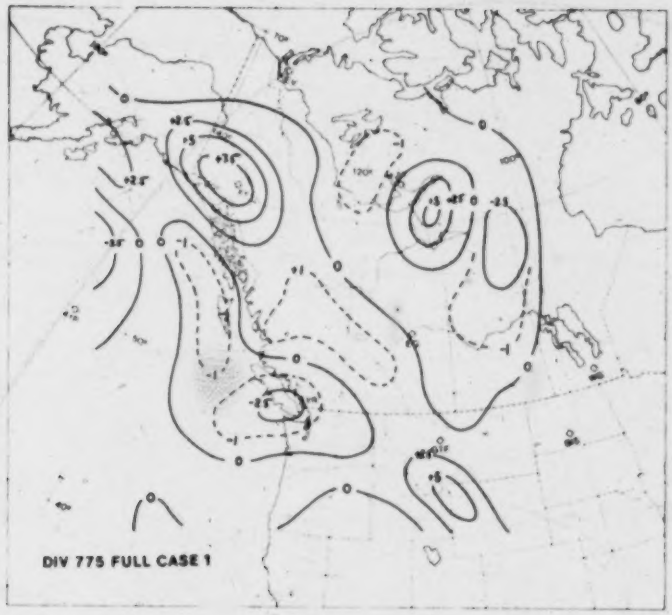

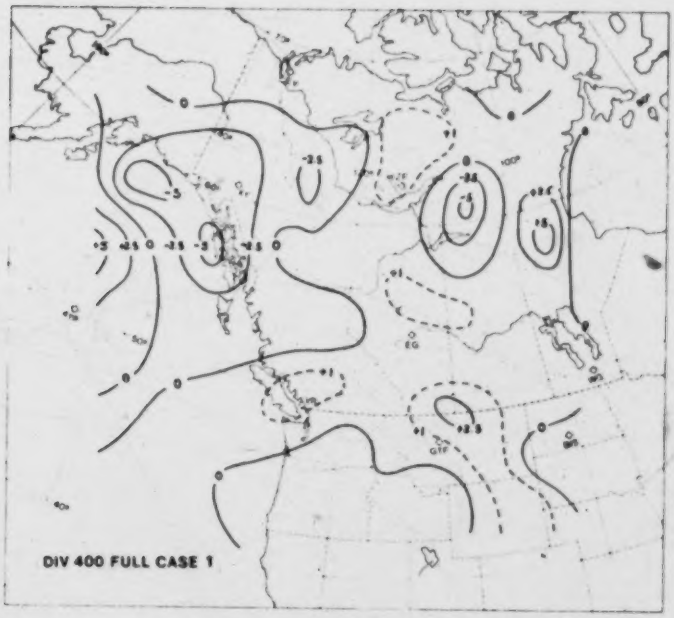

Fig. 12. Analysis of the divergence term (DIV) at 775 mb and 400 mb for the full lower boundary condition. Units are 2.8×10^{-10} sec^{-2}.

Alaska low and over Lake Athabasca. Since these two areas are associated with low level ascent, a compensating divergence should be expected aloft. The 400 mb divergence analysis confirms this, with divergence present over both areas. In general, the mean value of the divergence term is approximately double that of the tilting term when the mean is calculated over the entire grid.

Figure 13 shows the analyses of the sum of the tilting and the divergence terms (TILT + DIV) at 775 mb for both boundary conditions. Significant differences are noticeable in these two analyses. For the full boundary case, vorticity production increases up to 30 percent over the Yukon. On the west coast where vorticity was increasing with time in the simple boundary case, a change of sign occurs when the full boundary is included; the inclusion of the full boundary leads to decreasing vorticity in that area. Tables 3 to 5 list the mean values of the individual baroclinic terms and their sum by test area for both boundary conditions.

For each test area these tables demonstrate the same result: to the lee of the mountains, vorticity production is enhanced through inclusion of the full boundary; on the windward slopes of the Cordillera vorticity production is inhibited when the full boundary is included. These results agree with the findings of McClain (1960) and others. Note that in Area 4, relatively minor differences appear in the values of the baroclinic terms, again a result of the relatively even terrain in that area.

When the full boundary is included, two major results were obtained for this case. These are: (1) marked changes in omega

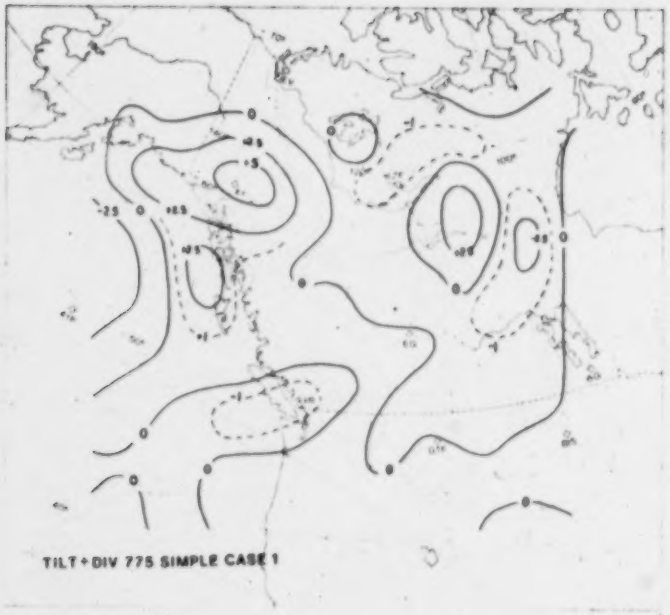

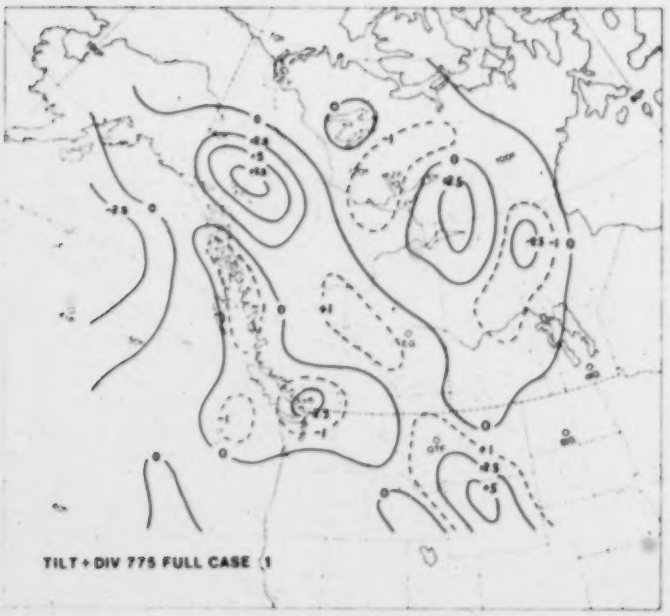

Fig. 13. Analysis of the sum of the tilting term and the divergence term at 775 mb for both lower boundary conditions. Units are 3.3×10^{-10} sec^{-2}.

Area	Level (mb)	Full Boundary	Simple Boundary
1	775	-0.3	-0.6
	600	-0.5	-0.4
	400	+0.1	+0.1
2	775	-1.2	-1.2
	600	-2.3	-2.4
	400	-1.7	-1.6
3	775	-0.9	-0.3
	600	+0.4	+0.7
	400	-0.04	-0.01
4	775	+0.3	+0.2
	600	-0.4	-0.4
	400	-0.2	-0.3

Table 3. Mean grid point values of the tilting term for each test area. Units are 10^{-10} sec^{-2}.

Area	Level (mb)	Full Boundary	Simple Boundary
	775	+0.3	-0.7
1	600	+1.6	+0.8
	400	-1.1	+0.6
	775	+7.6	+7.8
2	600	+0.5	+0.6
	400	-6.0	-6.1
	775	-0.7	+0.8
3	600	-1.2	-0.8
	400	-1.2	-0.9
	775	+1.8	+1.7
4	600	-0.3	-0.6
	400	-1.2	-1.7

Table 4. Mean grid point values of the divergence term for each test area. Units are 10^{-10} sec^{-2}.

Area	Level (mb)	Full Boundary	Simple Boundary
	775	0.0	-1.2
1	600	+1.2	+0.4
	400	+1.2	+0.7
	775	+6.4	+6.7
2	600	-1.8	-1.8
	400	-7.7	-7.5
	775	-1.6	+0.5
3	600	-0.8	-0.1
	400	-1.2	-0.9
	775	+2.2	+2.0
4	600	-0.7	-1.0
	400	-1.5	-2.0

Table 5. Mean grid point values for the sum of the tilting term and the divergence term for each test area. Units are 10^{-10} sec^{-2}.

values at 775 mb,but little change in the basic vertical motion pattern and (2) enhancement of vorticity production to the lee of the Rocky Mountains, accompanied by inhibition of vorticity production windward of the Rockies. The next two cases, although presented in lesser detail, demonstrate the same effects.

5.3 Case 2 (05 March 1972: 1200 GMT)

The results of this case are presented in Figures 14 to 19 and in Table 6. Figure 14 shows the surface analysis and the 500 mb geopotential height analysis for this case. At the surface, a well developed frontal wave (associated with a 992 mb low) was just over Vancouver Island at analysis time. The system was moving northeastward. Unlike Case 1, this system approached Alberta from the southwest. At 500 mb a southwesterly flow prevailed over the eastern Pacific Ocean and B.C. to a ridge along the B.C.-Alberta border. The flow was northwesterly over Alberta. Although not shown on the 500 mb analysis, significant PVA was present from Vancouver Island to east central B.C. A second area of PVA was located along a line from southern Idaho to southern Alberta. A significant area of negative vorticity advection (NVA) was situated along a line from Puget Sound to just west of Edmonton. At 850 mb (not shown) warm air advection associated with the frontal wave was located over Washington and southern B.C. An area of weak warm air advection, associated with the front in Alberta, stretched from northeastern B.C. to southern Saskatchewan. Twenty four hours after analysis time a 985 mb low was established 200 km east of Calgary. Careful

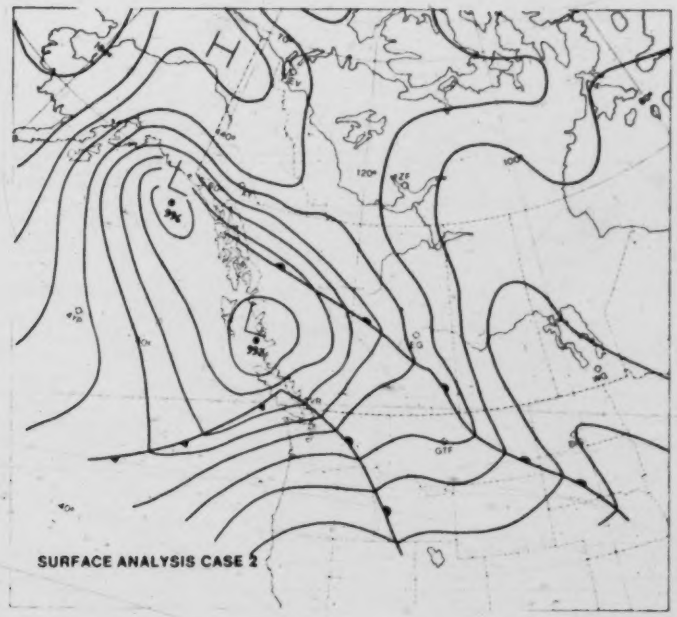

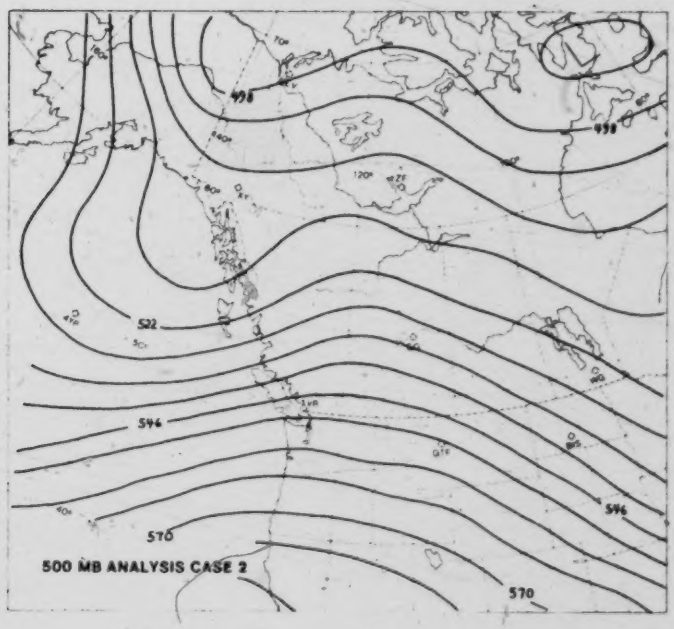

Fig. 14. Surface analysis and 500 mb geopotential height analysis for Case 2 (05 March 1972, 1200 GMT).

inspection of the meteorological charts for this 24 hour period did not conclusively show that a new low developed east of Calgary; more certainly the existing 992 mb low over Vancouver Island moved inland and deepened significantly upon crossing the Rocky Mountains.

The top half of Figure 15 shows the analyzed vertical motion at the earth's surface. A weak area of ascent predominates over the eastern Pacific Ocean due to the cyclonic circulation in that area; ascent over Vancouver Island is due mainly to upslope flow. Weak subsidence prevails to the lee of the Rocky Mountains.

Figure 16 shows the vertical motion pattern at 775 mb for the two lower boundary conditions. Little difference is noticeable between the two charts, although ascent over Vancouver Island is in fact enhanced 20 percent near the centre of this area when the full lower boundary is incorporated. The small ascent areas over Idaho and Montana decreased in intensity when the full boundary was included. As in Case 1, similar but weaker changes occurred in the 600 and 400 mb vertical motion fields upon inclusion of the full lower boundary. Figure 17 shows the 600 and 400 mb vertical motion patterns obtained using the full lower boundary.

The vertical motion fields agreed quite well with the reported weather phenomena. A large area of snow in B.C. and the Yukon coincided with the ascent patterns portrayed in Figures 15 to 17. Generally clear skies over northern Alberta verify the mid level subsidence over that area. The satellite photograph for this case (Figure 18) correlates well with the analyzed vertical motion fields.

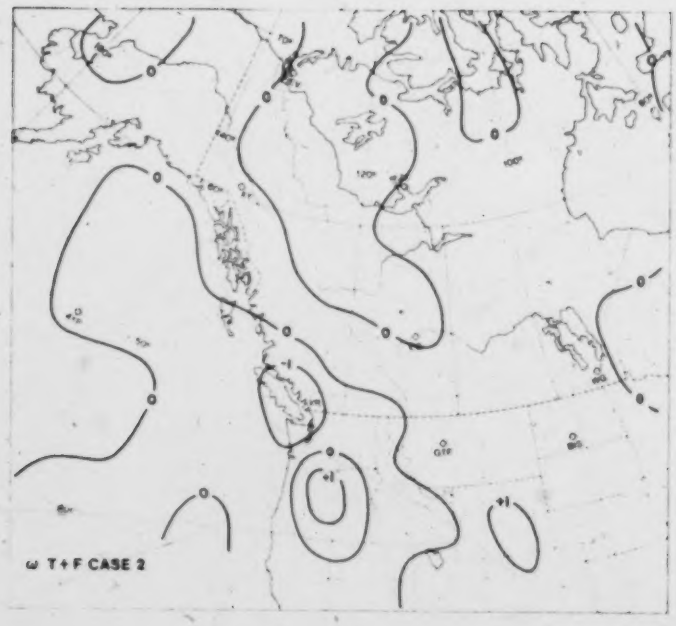

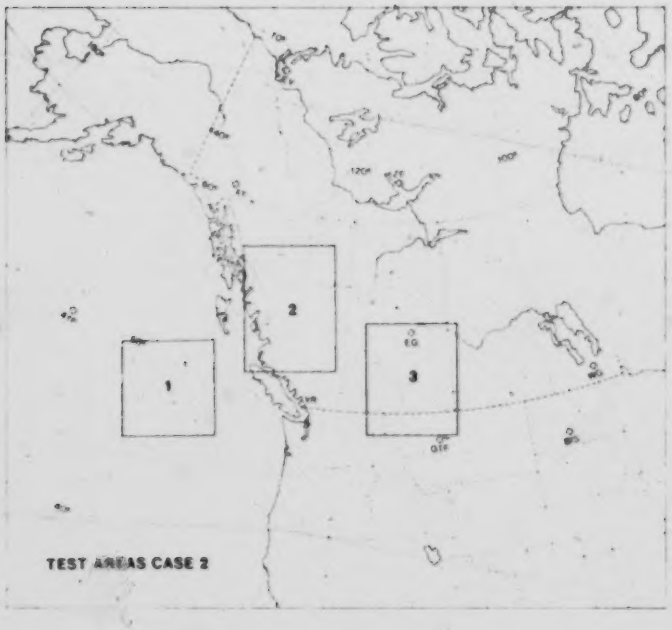

Fig. 15. Vertical motion at the earth's surface and the test areas used for comparison of the baroclinic terms of the vorticity equation.

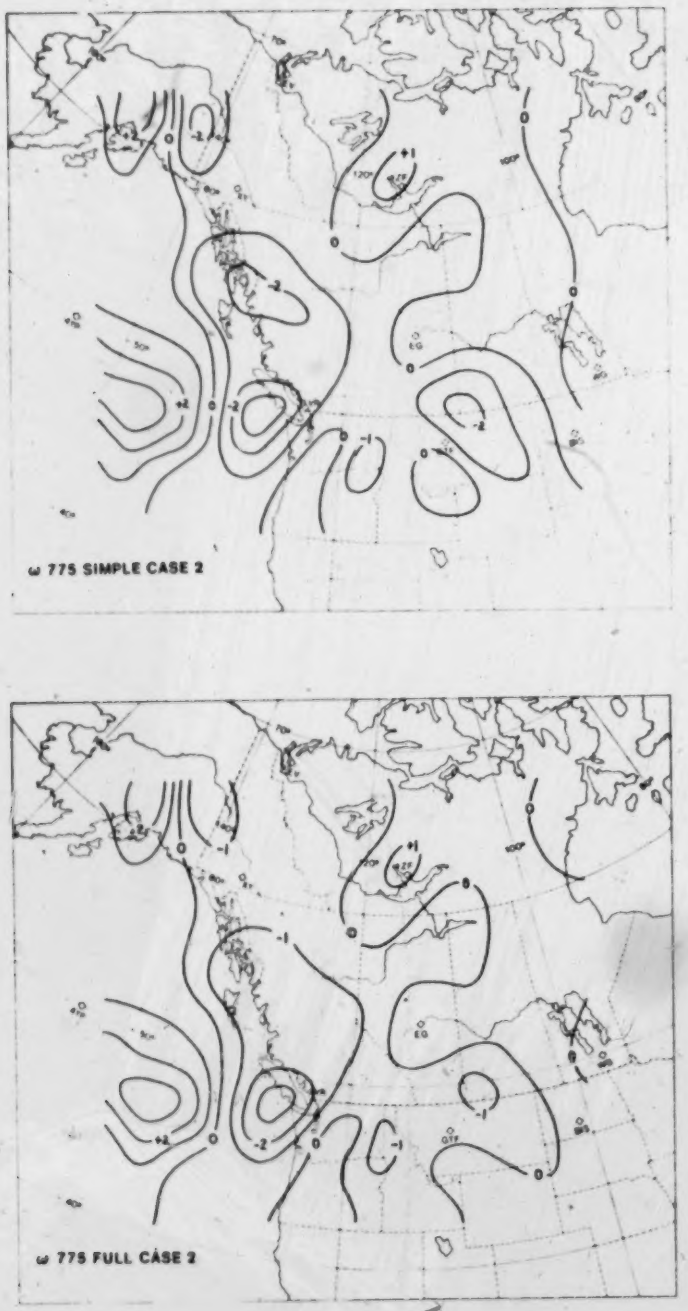

Fig. 16. Vertical motion patterns at 775 mb for the two lower boundary conditions.

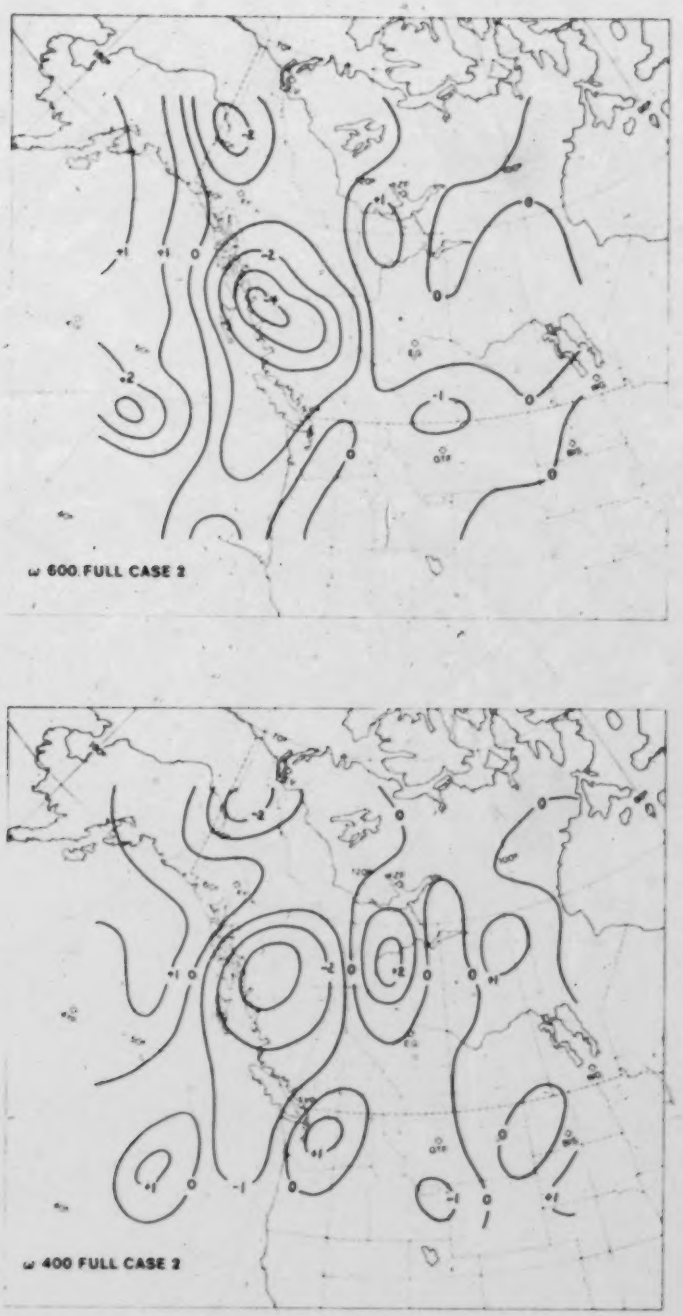

Fig. 17. Vertical motion patterns at 600 mb and 400 mb for the full lower boundary condition.

Fig. 18. Satellite photograph of the meteorological conditions for Case 2. Vancouver Island lies beneath the white cloud mass at the right centre of the photograph, with the Alaskan Panhandle visible as a bright band above Vancouver Island. A second band of cloud is situated just west of the Panhandle. The photograph was taken about 2000 GMT, 05 March 1972 by ESSA-8.

The sum of the baroclinic terms at 775 mb for the two different boundary conditions are present in Figure 19. Two maxima in vorticity production occur: one over central B.C., and a second area over Montana. These analyses also indicate that parcel vorticity is decreasing with time along the front in northern and eastern Alberta. Vorticity production over the eastern slopes of the Rockies increased noticeably when the full boundary was included. Vorticity production also increased in central B.C.; inspection of the terrain heights (Figure 4) shows that this area is to the lee of the Coast Range.

The test areas used for comparison of the baroclinic terms (Figure 15, bottom half) were chosen on the same basis as in Case 1. Area 1 is located west of Vancouver Island, where parcel vorticity is decreasing with time. Area 2 is located over the significant vorticity production zone in central B.C. Area 3 is located where the 985 mb low appeared 24 hours later, in the lee of the Rocky Mountains.

Table 6 compares the mean values of the baroclinic terms over the test areas for the two boundary conditions. The results are in agreement with those of Case 1. Vorticity production is enhanced to the lee of mountain barriers and inhibited on the windward side when the full boundary is included. The vorticity production areas are not in the same locations as in Case 1. This suggests that orientation of the mid level atmospheric flow to the mountain barrier may be an important factor in lee cyclogenesis.

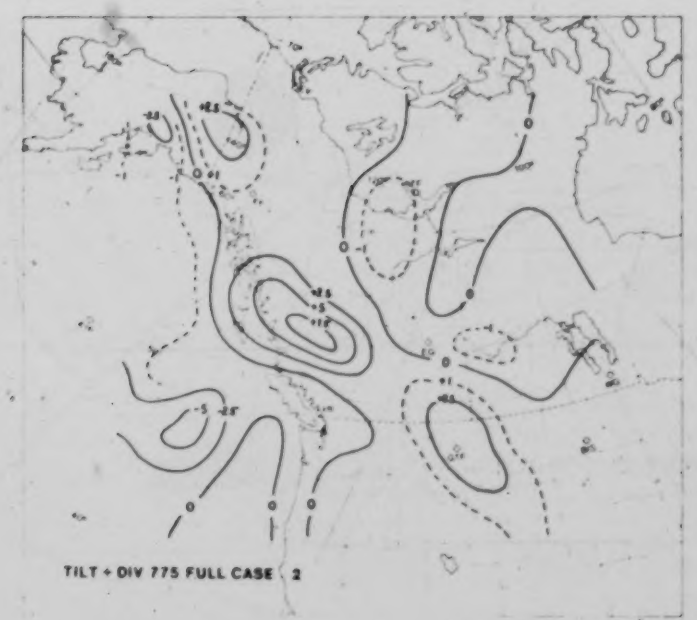

Fig. 19. Sum of the tilting term and the divergence term at 775 mb for the two lower boundary conditions. Units are 3.0×10^{-10} sec^{-2}.

Area	Level (mb)	Full Boundary	Simple Boundary
	775	-6.0	-5.3
1	600	+6.4	+6.7
	400	+2.4	+2.6
	775	+8.9	+8.3
2	600	+3.8	+3.6
	400	-7.9	-8.2
	775	+2.8	+2.2
3	600	-1.9	-2.6
	400	-0.9	-1.3

Table 6. Case 2 mean grid point values for the sum of the tilting term and the divergence terms for each test area. Units are 10^{-10} sec^{-2}.

5.4 Case 3 (21 May 1972: 1200 GMT)

The results for this case are presented in Figures 20 to 25, and in Table 7. Case 3 differs significantly from Case 1 and Case 2. Although a low pressure system developed in northwestern Alberta, the large scale circulation features of the atmosphere were changing as well. At analysis time at 996 mb, a low pressure system (see Figure 20) was situated over northern B.C. The system moved eastward to just south of Great Slave Lake in 24 hours, deepening only to 992 mb. At 500 mb the flow was weak over Alberta and B.C. A trough extended from a low situated over the Gulf of Alaska to a second low over Idaho. This entire system moved inland to the lee of the Rocky Mountains in 12 to 24 hours. PVA was situated over the Alaskan Panhandle, but at the same time, cold air advection was present in the same area. Another area of PVA was located over the Mackenzie Mountains. This PVA together with warm air advection at 700 mb (not shown) is a good combination for producing ascent.

Figure 21 (top half) shows the analysis of vertical motion at the earth's surface. A general pattern of weak ascent is prevalent west of the Continental Divide. An area of weak subsidence appears over the southern Yukon and the southern Mackenzie Valley. Another area of weak ascent located near Bismarck, North Dakota (BIS) is associated with the upslope flow in that area.

Figure 22 shows the analyzed vertical motion patterns at 775 mb for the two lower boundary conditions. Very little difference is apparent between these analyses, as the vertical motion at the earth's surface is generally weak in this case. Some changes are

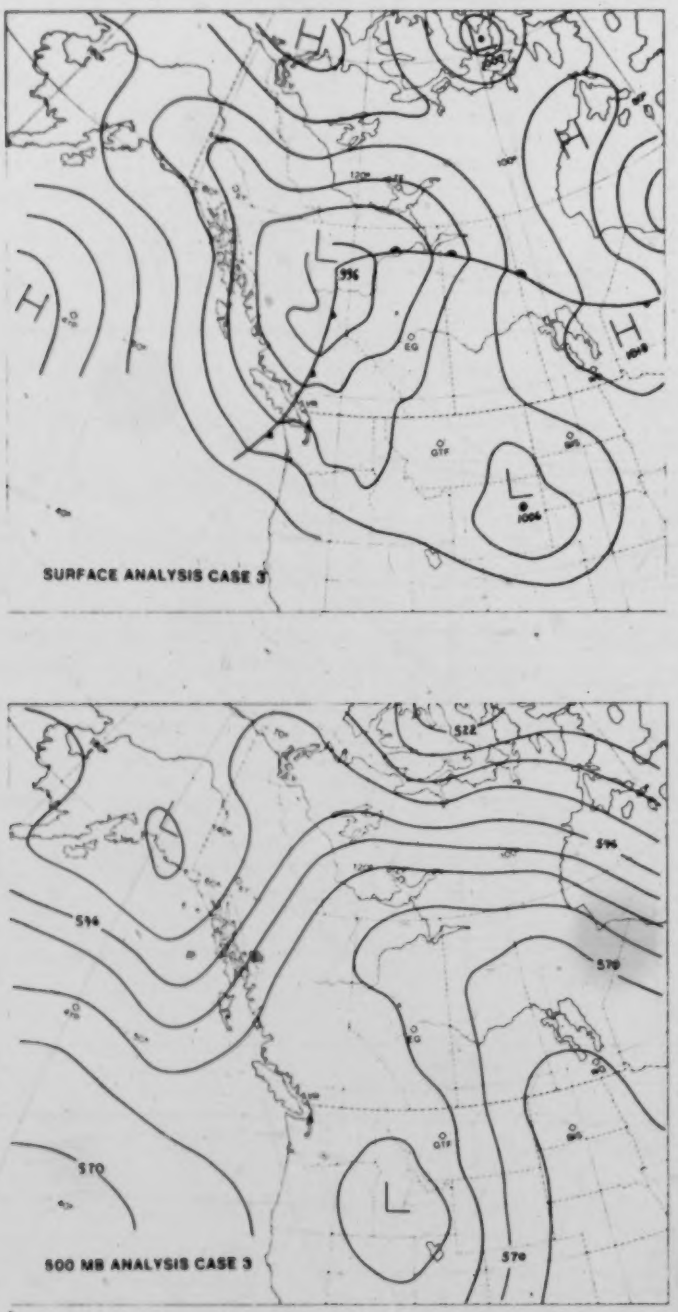

Fig. 20. Surface analysis and 500 mb geopotential height analysis for Case 3 (21 May 1972, 1200 GMT).

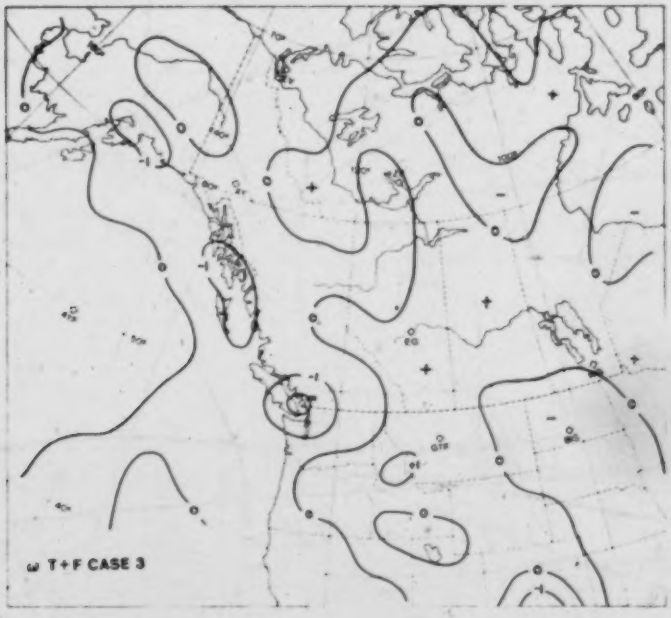

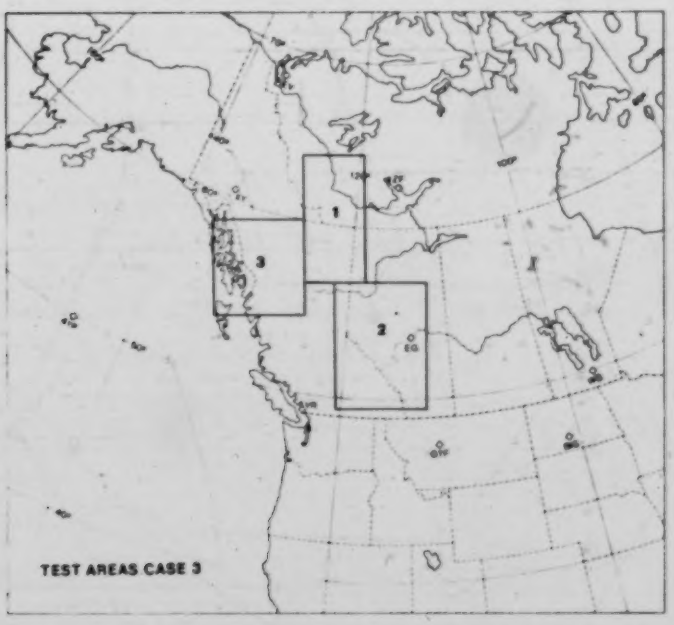

Fig. 21. Vertical motion at the earth's surface and the test areas used for comparison of the baroclinic terms of the vorticity equation.

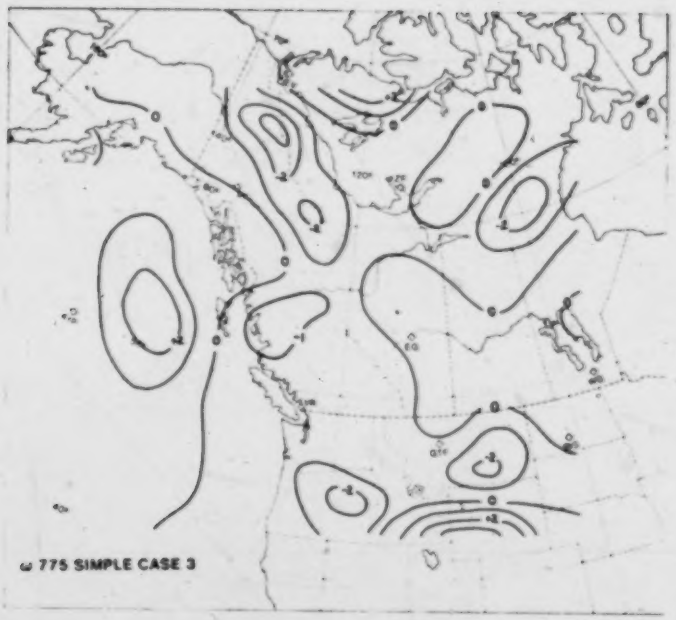

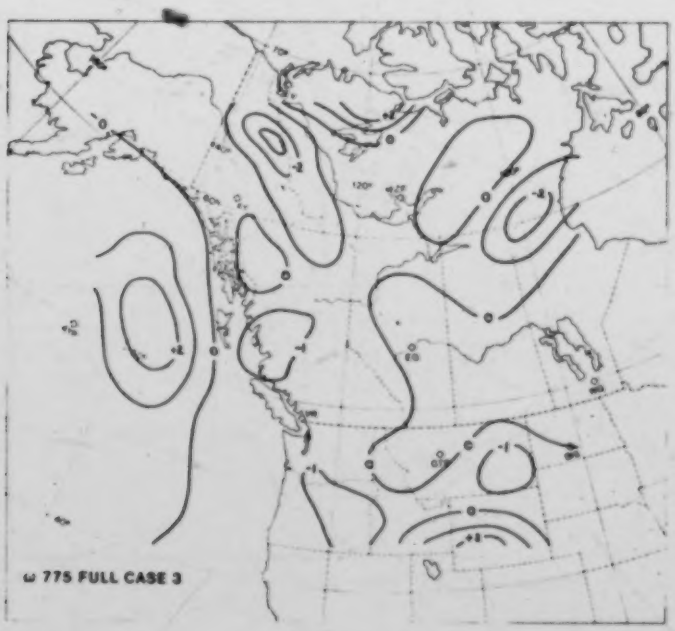

Fig. 22. Vertical motion patterns at 775 mb for the two lower boundary conditions.

apparent in the small ascent areas in the northwestern U.S. The area of ascent over the Mackenzie Mountains is in response to PVA and warm air advection, as mentioned earlier. The vertical motion fields at the 600 and 400 mb levels are presented in Figure 23.

Reported surface weather phenomena did not correlate particularly well with the derived vertical motions in this case. However, the satellite photograph of the weather pattern (Figure 24) taken some eight hours after analysis time, did show organized cloud patterns in the ascent areas.

Figure 25 shows the analysis of the baroclinic terms at 775 mb for the two lower boundary conditions. Some differences are noticeable between the two analyses. A small area of vorticity production appears southwest of Edmonton in the full boundary case. Major changes occur in the vorticity production pattern associated with the system over the northwestern U.S., but little change is apparent in the vorticity production area over the Mackenzie Mountains. When the mean values of the baroclinic terms are considered for the test areas (Figure 21, bottom half), it is evident that vorticity production is enhanced to the lee of the mountains and inhibited windward of these barriers when the full boundary is introduced. The mean values of the baroclinic terms are shown in Table 7.

5.5 Summary

In all three cases, the derived vertical motion patterns agreed reasonably well with the observed weather phenomena at or

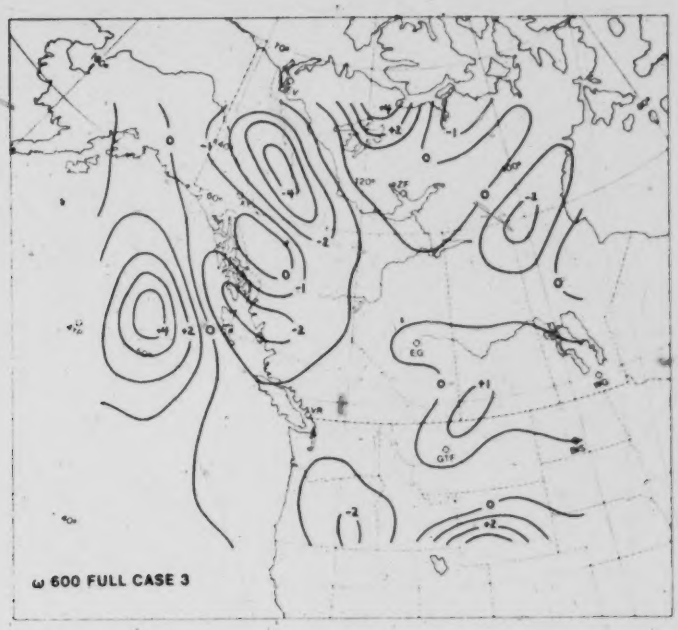

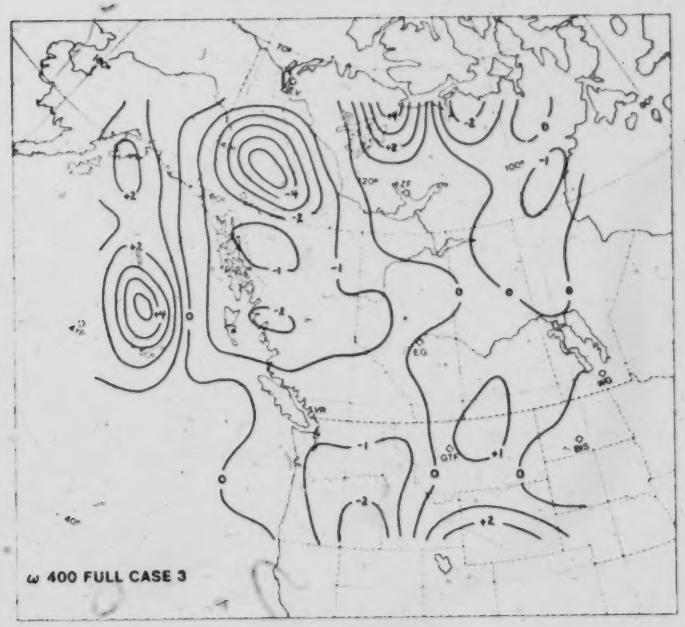

Fig. 23. Vertical motion patterns at 600 mb and 400 mb for the full lower boundary condition.

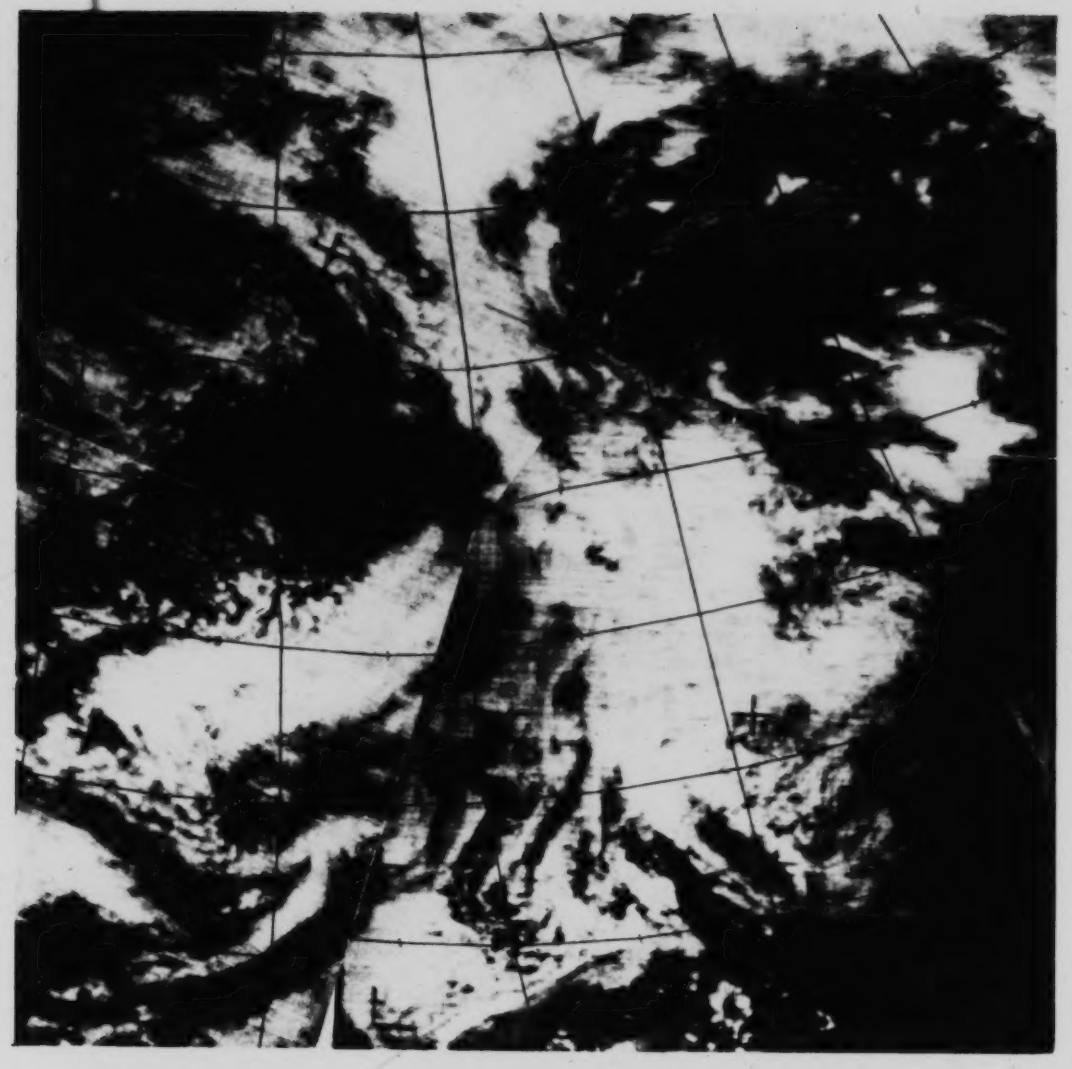

Fig. 24. Satellite photograph mosaic of the meteorological conditions for Case 3. This photograph was available in specially prepared gridded format, thanks to Mr. D. L. Oracheski, a graduate student at the University of Alberta. Longitude lines are every 10° and latitude lines every 5°. 60N, 120W is just southwest of Great Slave Lake (plainly visible).

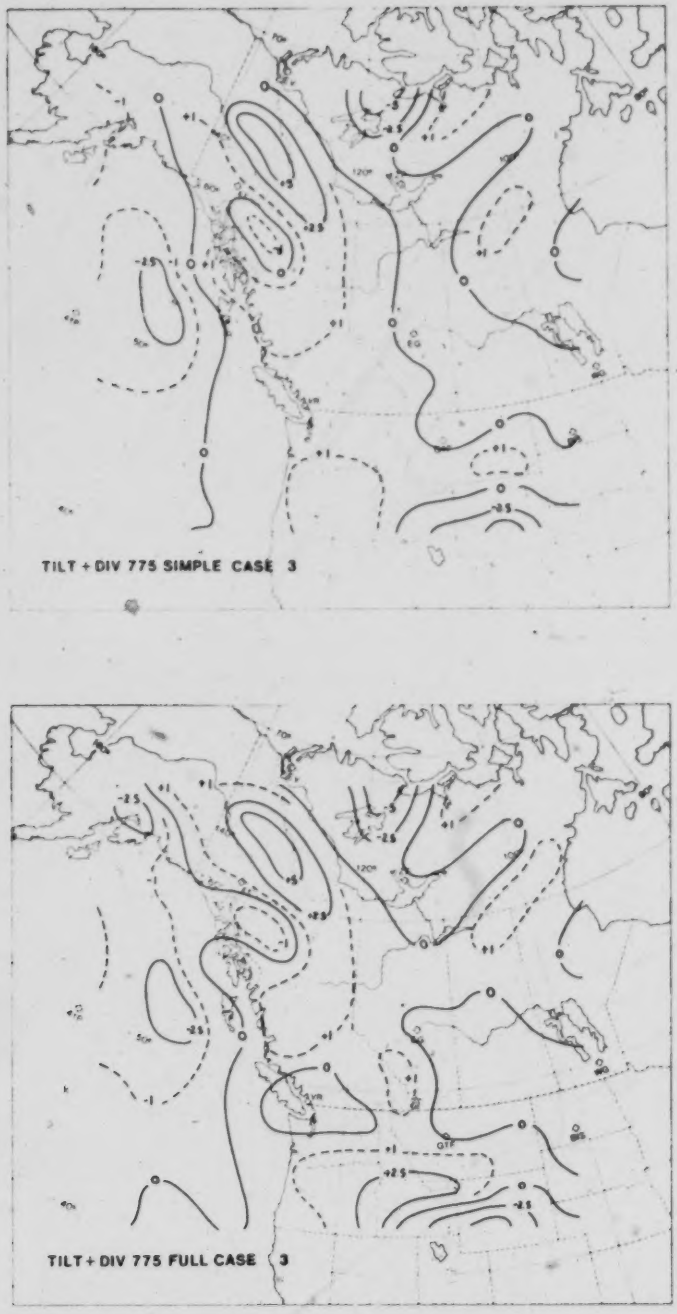

Fig. 25. Sum of the tilting term and the divergence term for the two lower boundary conditions. Units are 3.5×10^{-10} sec^{-2}.

Area	Level (mb)	Full Boundary	Simple Boundary
	775	+3.5	+3.1
1	600	-0.8	-1,1
	400	-1.2	-1.3
	775	+1.5	+1.0
2	600	+1.9	+1.8
	400	-0.9	-1.0
	775	+2.2	+3.1
3	600	+2.9	+3.2
	400	-2.5	-2.3

Table 7. Case 3 mean grid point values for the sum of the tilting term and the divergence term for each test area. Units are 10^{-10} sec^{-2}.

near the analysis time. Differences of up to 30 percent in the vertical motion values appear at 775 mb when the full lower boundary is included in the solution of the omega equation; however, the major features of the vertical motion patterns do not alter significantly. A similar difference in vertical motion values appears at 600 and 400 mb but to a lesser extent than at 775 mb. Introduction of the full lower boundary in the model indicates that a major mountain barrier induces vorticity production to its lee and inhibits the vorticity production to the windward side.

CHAPTER VI

SUMMARY AND CONCLUSIONS

In this study a four level model of the atmosphere was formulated to obtain the three dimensional vertical velocity fields by solution of the quasi-geostrophic omega equation. The omega equation was solved numerically over a grid encompassing western Canada, most of the Northwest Territories, Alaska and parts of the eastern Pacific Ocean. A grid with 21 rows and 23 columns was constructed and a grid distance of 200 km was used in the x and y direction. Three synoptic situations were chosen from which input data at various levels were constructed using an objective analysis scheme. Data from Lark Juliet flights were utilized to improve the data coverage over the Pacific Ocean. In addition, synthetic data were introduced over areas of inadequate coverage in order to improve the accuracy of the objective analysis scheme.

In the solution of the omega equation, two different lower boundary conditions were used. The first, a simple lower boundary consisted of a flat, frictionless surface and was represented by zero vertical velocity everywhere. The second boundary condition incorporated the analyzed station pressures and observed

winds at the earth's surface, along with carefully evaluated terrain heights and drag coefficient data. Using this information, the values of orographically and frictionally induced vertical motion at the earth's surface were calculated and applied at the station pressure level in the model atmosphere, forming a realistic lower boundary condition. For quantitative assessment, the divergence and the tilting terms of the vorticity equation were evaluated over selected test areas using the two different boundary conditions.

The results of applying the realistic lower boundary condition compared to the simple lower boundary condition were twofold. Firstly, the values of omega at 775 mb changed by as much as 30 percent, with diminishing changes at higher levels. These changes in turn augmented the patterns of the divergence and the tilting terms of the vorticity equation, enhancing vorticity production to the lee of major mountain barriers in western Canada while inhibiting vorticity production on the windward side. Through a detailed analysis of these terms specific areas of enhanced vorticity production were noted. For the three synoptic situations studied here, it appears that these vorticity production areas could be correlated to known areas of cyclogenesis in the lee of the western Cordillera.

This study further revealed that low level vorticity production was enhanced in areas of orographic descent due mainly to low level convergence. These findings are in broad agreement with an earlier study (Chung, 1972) which concludes that "most lee cyclones formed initially under the eastern margin of a 500 mb

orographically intensified diffluent cross barrier flow superimposed on a zone of low level convergence and orographic descent."

This study has brought out the importance of orography and surface friction on vorticity production which may provide a link in the formation of cyclones to the lee of the Canadian Rockies. These results may prove to be important towards development of a suitable prediction model for weather systems over western Canada.

LIST OF SYMBOLS

C_D	drag coefficient
d	finite difference grid interval
f	Coriolis parameter
g	acceleration of gravity
G	forcing function in the omega equation
h	terrain height above mean sea level
$\vec{k}$	unit vector in the (local) vertical
m	map factor
p	atmospheric pressure
p_g	pressure at the earth's surface
R	radius of influence
R_d	specific gas constant of dry air
R_{ij}	residual at grid point i,j
t	time
u	east-west component of the wind (x-axis points east)
v	north-south component of the wind (y-axis points north)
V	magnitude of the wind
$\vec{V}$	horizontal wind vector
$\vec{V}_g$	geostrophic wind vector
Z	geopotential height
α	specific volume
ζ	relative vorticity = $\vec{k} \cdot \nabla \times \vec{V}$
η	absolute vorticity
θ	potential temperature
ρ	density of the air

σ	$= -\frac{\alpha}{\theta}\frac{\partial \theta}{\partial p}$, a measure of static stability
τ_{zx}, τ_{zy}	x and y components of the shear stress in the xy plane
ω	$= \frac{dp}{dt}$ = vertical velocity expressed in terms of pressure
ω_f	frictionally induced vertical velocity at the earth's surface
ω_g	sum of frictionally and orographically induced vertical motion at the earth's surface
ω_t	orographically induced vertical motion at the earth's surface
o	subscript which unless otherwise indicated denotes the earth's surface

OPERATORS

$\frac{\partial}{\partial p}$	the differential operator along the p-axis
$\frac{\partial}{\partial x}$	the differential operator along the x-axis
$\frac{\partial}{\partial y}$	the differential operator along the y-axis
∇	the two dimensional gradient operator
∇^2	the two dimensional Laplacian operator
ϕ^2	the finite difference form of the two dimensional Laplacian operator
J(,)	the Jacobian operator

STATION IDENTIFIERS

BA	Banff, Alberta
BIS	Bismarck, North Dakota
BK	Baker Lake, Northwest Territories (NWT)
CB	Cambridge Bay, NWT
DL	Dease Lake, B.C.
EG	Edmonton, Alberta
EI	Ennadai Lake, NWT
EV	Inuvik, NWT
FAI	Fairbanks, Alaska
GTF	Great Falls, Montana
JA	Jasper, Alberta
MM	Fort McMurray, Alberta
QR	Regina, Saskatchewan
SM	Fort Smith, NWT
VQ	Norman Wells, NWT
VR	Vancouver, B.C.
WO	Contwoyto Lake, NWT
XE	Saskatoon, Saskatchewan
XJ	Fort St. John, B.C.
XS	Prince George, B.C.
XY	Whitehorse, Yukon Territory
YE	Fort Nelson, B.C.
YQ	Churchill, Manitoba
ZF	Yellowknife, NWT
4YP	Ocean Station Papa, 50N, 145W

BIBLIOGRAPHY

Aubert, E.J., 1957: On the release of latent heat as a factor in large scale atmospheric motions. J. Meteor., 14, pp. 527-542.

Bergthorsen, P., and Döös, B., 1955: Numerical weather map analysis. Tellus, 7, pp. 329-340.

Chung, Y.S., 1972: Cyclogenesis in the lee of the Canadian Rocky Mountains. M.Sc. Thesis, Univ. of Alberta.

Cressman, George P., 1959: An operational objective analysis system. Mon. Wea. Rev., 87, pp. 367-374.

_____ , 1960: Improved terrain effects in barotropic forecasts. Mon. Wea. Rev., 88, pp. 327-342.

_____ , 1963: A three level model suitable for daily numerical forecasting. National Meteorological Centre Technical Memorandum No. 22, U.S. Department of Commerce, Weather Bureau, Washington, D.C., 22 pp.

Danard, Maurice B., 1964: On the influence of released latent heat in cyclone development. J. Appl. Meteor., 3, pp. 27-37.

_____ , 1966: A quasi-geostrophic numerical model incorporating effects of release of latent heat. J. Appl. Meteor., 5, pp. 85-93.

_____ , 1969: Numerical studies of the effect of surface friction on large scale atmospheric motion. Mon. Wea. Rev., 97, pp. 835-844.

Fjørtoft, R., 1955: On the use of space smoothing in physical weather forecasting. Tellus, 7, pp. 462-480.

Gates, W.L., 1961: Static stability measures in the atmosphere. J. Meteor., 18, pp. 526-533.

Glahn, H.R. and Hollenbaugh, G.W., 1969: An operationally oriented small-scale 500-millibar height analysis program. U.S. Department of Commerce, Essa Technical Memorandum WBTM TDL 19, 18 pp.

Glahn, H.R., Hollenbaugh, G.W., and Lowery, D.A., 1969: An operationally oriented objective analysis program. U.S. Department of Commerce, Essa Technical Memorandum WBTM TDL 22, 20 pp.

Graystone, P., 1962: The introduction of topographic and frictional effects in a baroclinic model. Quart. J. Roy. Meteor. Soc., 88, pp. 256-270.

Haltiner, G.J., Clarke, L.C., and Lawniczak, G.E., 1963: Computation of the large scale vertical velocity, J. Appl. Meteor., 2, pp. 242-259.

Haltiner, G.J., 1971: Numerical weather prediction. John Wiley and Sons, Inc., N.Y. and Toronto, 317 pp.

Lorenz, E.N., 1955: Available potential energy and the maintenance of the general circulation. Tellus, 7, pp. 157-167.

_____, 1960: Energy and numerical weather prediction. Tellus, 12, pp. 364-373.

McClain, E. Paul, 1960: Some effects of the western Cordillera of North America on cyclone activity. J. Meteor., 7, pp. 104-115.

Miller, Albert, and Panofsky, H.A., 1958: Large scale vertical motions and weather in January, 1953. Bull. Amer. Meteor., Soc., 39, pp. 8-13.

Mogil, H. Michael, and Holle, Ronald L., 1972: Anomalous gradient winds : existence and implications. Mon. Wea. Rev., 10, pp. 709-716.

Newton, C.W., 1956: Mechanisms of circulation change during a lee cyclogenesis. J. Meteor., 13, pp. 528-539.

O'Neill, Thomas H.R., 1966: Vertical motions and precipitation computations. J. Appl. Meteor., 5, pp. 595-605.

Panofsky, H.A., 1946: Methods of computing vertical motions in the atmosphere. J. Meteor., 3, pp. 45-49.

Richardson, L.F., 1922: Weather prediction by numerical processes. Reprint, Dover Publications, N.Y., 236 pp.

Sawyer, J.S., 1959: The introduction of the effects of topography into methods of numerical forecasting. Quart. J. Roy. Meteor. Soc., 85, pp. 31-43.

Smagorinsky, J., and Collins, G.O., 1955: On the numerical prediction of precipitation. Mon. Wea. Rev., 83, pp. 53-68.

Smebye, Sigurd F., 1958: Computation of precipitation from large scale vertical motion. J. Meteor., 15, pp. 547-560.

Smith, Phillip J., 1971: An analysis of kinematic vertical motions. Mon. Wea. Rev., 99, pp. 715-724.

Stuart, David W., 1964: A diagnostic case study of the synoptic scale vertical motion and its contribution to mid-tropospheric development. J. Appl. Meteor., 3, pp. 669-684.

_____, and O'Neill, Thomas H.R., 1967: The over-relaxation factor in the numerical solution of the omega equation. Mon. Wea. Rev., 95, pp. 303-307.

Thompson, P.D., 1961: Numerical weather analysis and prediction. MacMillan and Co., N.Y., 166 pp.

Whitehead, Victor S., 1965: Synthesis of 500-mb height and temperature data by consideration of surface pressure and temperature and the behaviour of density with height. Mon. Wea. Rev., 93, pp. 559-564.